

Measurement and modelling of homogeneous axisymmetric turbulence

By TORBJÖRN SJÖGREN
AND ARNE V. JOHANSSON

Department of Mechanics, KTH, SE-100 44 Stockholm, Sweden

(Received 28 April 1997 and in revised form 26 May 1998)

A new method for determining the slow and rapid pressure–strain rate terms directly from wind-tunnel experiments has been developed with the aid of a newly developed theoretical description of the kinematics of homogeneous axisymmetric turbulence. Both the straining and the return-to-isotropy process of homogeneous axisymmetric turbulence are studied with the aim of improving Reynolds stress closures. Direct experimental determination of the different terms in the transport equation for the Reynolds stress tensor plays a major role in the validation and development of turbulence models. For the first time it is shown that the pressure–strain correlation can be determined with good accuracy without balancing it out from the Reynolds stress transport equation (and without measuring the pressure). Instead it is determined through evaluation of integrals containing second- and third-order two-point velocity correlations. All the terms in the Reynolds stress equations are measured directly and balance is achieved.

1. Introduction

Axisymmetric turbulence is the simplest type of turbulence where redistribution of energy, related to pressure–strain and anisotropic dissipation, exists. The lowest level of turbulence models at which such effects enter explicitly is that in which transport equations are formulated for the individual Reynolds stress components. To study these effects experimentally we have generated nearly isotropic turbulence by a monoplane grid containing square rods, and used the axisymmetric straining field of the contraction in the MTL wind-tunnel at KTH. In this way highly anisotropic axisymmetric turbulence was generated at the beginning of the test section. The straining also ensures a very good homogeneity of the flow.

The theory of axisymmetric turbulence was first analysed by Batchelor (1946) followed by Chandrasekhar (1950) and recently by Lindborg (1995). Lindborg used a representation that makes use of the ‘cylindrical’ symmetry properties and considerably simplified the earlier theory which used a representation more suited to the isotropic ‘spherical’ case. He was also able to derive new explicit relations for the pressure–strain correlations as integrals over measurable two-point velocity correlations. This formalism was utilized in the present experimental investigation of intercomponent transfer both in the straining phase and in the subsequent relaxation towards isotropy.

The use of grids in a uniform stream to generate turbulence may be said to have begun with the work of Simmons & Salter in 1934 and was used the year after by Taylor (1935*b*) who proposed a linear decay law for the streamwise energy

component. Theoretical work on the isotropic turbulence problem was also presented by von Kármán & Howarth (1938) for the ‘final period of decay’. Experimental studies of the dynamics and the decay of isotropic turbulence were later conducted by e.g. Batchelor & Townsend (1947, 1948) Grant & Nisbet (1957), Frenkiel & Klebanoff (1971) among others.

It is also well known that grid-generated turbulence has slightly higher energy content in the streamwise component compared to the lateral ones. Comte-Bellot & Corrsin (1966) used a small contraction in order to account for that effect and produce nearly isotropic turbulence. Their results have been used for modelling purposes in numerous investigations, e.g. by Lumley & Newman (1977) to define asymptotic conditions as the anisotropy becomes small.

The effect of the straining field in an axisymmetric contraction on turbulence is of interest both to the wind-tunnel designer and the turbulence theoretician. The historical development of the theory of turbulence passing a contraction appears to have begun with the ideas of Prandtl (1930) and was extended by Taylor (1935*a*), who addressed the already, at that time, well known effect that a contraction reduces the longitudinal fluctuations.

Experimental studies of axisymmetric strained turbulence began with the measurements of Uberoi (1956, 1957), followed by Hussain & Ramjee (1976) who investigated the influence of different axisymmetric contraction shapes. Warhaft (1980) was able to incorporate thermal fluctuations in grid-generated turbulence in order to examine the effect of an axisymmetric strain on passive scalar fluctuations.

Experimentally, the return to isotropy of axisymmetric turbulence has been studied by Uberoi (1956, 1957), Warhaft (1980) and Groth, Hallbäck & Johansson (1989), who investigated grid-generated turbulence strained by the axisymmetric contraction of a wind tunnel. Choi (1983) was able to generate an axisymmetric expansion and a plane distortion in the wind tunnel by changing the inlet duct to the test section. Anisotropic turbulence after a plane distortion was also studied by Tucker & Reynolds (1968), and then by Gence & Mathieu (1980). Le Penven, Gence & Comte-Bellot (1985) used two different inlet ducts to generate an axisymmetric contraction and an expansion.

Most of these earlier studies are focused on the behaviour of the measured single-point Reynolds stress components to analyse the ‘return-to-isotropy’ problem. This approach is here extended to include two-point measurements. To better understand the energy redistribution process in the test section of the wind tunnel we here attempt to isolate the two parts of the ‘return-to-isotropy’ mechanism representing the viscous and pressure related effects. The two parts are extremely difficult to measure separately in a wind tunnel because of the several different velocity derivative moments contained in the total dissipation rate tensor and because of the difficulty of measuring pressure fluctuations. This split can, however, easily be performed on data from direct numerical simulations (DNS) where one can solve the Poisson equation for the fluctuating pressure, see e.g. Lee & Reynolds (1985), Mansour, Kim & Moin (1988) and Hallbäck, Sjögren & Johansson (1993). The task is much more difficult in a physical experiment.

In the present investigation the velocity is measured at two different points simultaneously in order to determine the two-point second- and third-order velocity correlations. This procedure gives us the possibility of determining all essential statistics and the kinematic behaviour of homogeneous axisymmetric turbulence, see Lindborg (1995).

Our objective here is to study the effect of axisymmetric strain, and the subsequent return towards isotropy when the strain is removed, in the context of Reynolds

stress closures. The primary quantities in Reynolds stress turbulence closures are the Reynolds stresses $\overline{u_i u_j}$ and the dissipation rate ε . The transport equations for these quantities can be written

$$\frac{D\overline{u_i u_j}}{Dt} = \mathcal{P}_{ij} + \Pi_{ij} - \varepsilon_{ij} - \frac{\partial J_{ijk}}{\partial x_k}, \quad (1.1)$$

$$\frac{D\varepsilon}{Dt} = \mathcal{P}^\varepsilon + T^\varepsilon - D^\varepsilon - \frac{\partial J_k^\varepsilon}{\partial x_k}. \quad (1.2)$$

The production term \mathcal{P}_{ij} can be explicitly expressed in the primary quantities and the mean velocity gradient tensor, and does not need to be modelled. All other terms depend on unknown correlations and require modelling. In order to separate amplitude and anisotropy related behaviour we here prefer to split the equation (1.1) into transport equations for the kinetic energy, $K = \frac{1}{2}\overline{u_i u_i}$, and the Reynolds stress anisotropy tensor, $a_{ij} = \overline{u_i u_j}/K - \frac{2}{3}\delta_{ij}$,

$$\frac{DK}{Dt} = \mathcal{P} - \varepsilon - \frac{\partial J_k}{\partial x_k}, \quad (1.3)$$

$$\frac{Da_{ij}}{Dt} = \mathcal{P}_{ij}^{(a)} + \frac{1}{K}(\Pi_{ij}^{(r)} + \Pi_{ij}^{(s)}) - \frac{\varepsilon}{K}(e_{ij} - a_{ij}) + \text{Diff}_{ij}^{(a)}, \quad (1.4)$$

where $\mathcal{P} = \frac{1}{2}\mathcal{P}_{kk}$ is the production of kinetic energy and $\varepsilon = \frac{1}{2}\varepsilon_{kk}$ is the total dissipation rate. In analogy with the Reynolds stress anisotropy tensor one defines the dissipation rate anisotropy tensor as

$$e_{ij} = \frac{\varepsilon_{ij}}{\varepsilon} - \frac{2}{3}\delta_{ij} \quad (1.5)$$

which is a part of the dissipative sink term in equation (1.4). This term is also determined directly from the two-point measurements.

The pressure–strain correlation, Π_{ij} , is normally split into a rapid part (r) that responds immediately to changes in the mean velocity gradient field, and a slow part (s) which is the part that remains in the absence of mean velocity gradients. For homogeneous turbulence the last (diffusion) term in equations (1.1) to (1.4) vanishes.

In the case of axisymmetric turbulence there is only one vector determining the overall symmetry and the Reynolds stress anisotropy tensor has only one independent component. We here let the symmetry axis be aligned with the x_1 -coordinate direction so that the off-diagonal components of a_{ij} are zero and $a_{22} = a_{33} = -\frac{1}{2}a_{11}$. The transport equations for the Reynolds stress anisotropy, the turbulent energy, and the total dissipation rate for the case of homogeneous axisymmetric turbulence then read

$$U \frac{da_{11}}{dx} = \mathcal{P}_{11}^{(a)} + \frac{1}{K}(\Pi_{11}^{(r)} + \Pi_{11}^{(s)}) - \frac{\varepsilon}{K}(e_{11} - a_{11}), \quad (1.6)$$

$$U \frac{dK}{dx} = \mathcal{P} - \varepsilon, \quad (1.7)$$

$$U \frac{d\varepsilon}{dx} = \mathcal{P}^\varepsilon + T^\varepsilon - D^\varepsilon. \quad (1.8)$$

The Taylor hypothesis is used to convert the time derivative to derivatives associated with the downstream position, as usual for studies of homogeneous axisymmetric turbulence in wind-tunnel experiments.

In order to close this set of transport equations one needs to express the unknown quantities, such as pressure–strain rate and dissipation rate anisotropy in terms of known quantities. This has been the topic of numerous investigations and is discussed in detail by Sjögren & Johansson (1997), where realizable nonlinear algebraic models are derived for both the dissipation rate anisotropy and the pressure–strain rate terms.

For an infinitely rapid strain we can see from (1.6) that the anisotropy state is determined by the action of the production term $\mathcal{P}_{ij}^{(a)}$ and the rapid pressure–strain rate $\Pi_{ij}^{(r)}$. In the absence of mean strain, on the other hand, the return-to-isotropy process is governed by the slow pressure–strain rate, $\Pi_{ij}^{(s)}$, and the anisotropy of the dissipation rate tensor, e_{ij} . In order to separate these effects in a situation with finite strain one has to be able to determine all of these different quantities.

The pressure–strain correlation has traditionally been regarded as unmeasurable. The technique for measuring the velocity by hot-wire anemometry is based on a macroscopic relation between the velocity surrounding the hot wire and its consequent cooling. Such a simple relation does unfortunately not exist for the fluctuating pressure. Any device which is put into a turbulent flow will naturally have a no-slip boundary condition. This will automatically create a fluctuating pressure field around the device which will be very complicated to measure. If one could solve this problem and measure the pressure fluctuation the task of relating the measured pressure fluctuation to that in the undisturbed flow would still be extremely difficult. To measure the fluctuating pressure in the interior of the flow is therefore more or less impossible.

The only way to determine the pressure–strain correlation has so far been to extract it from the balance of the transport equation for the Reynolds stress tensor by measuring all the other terms, see Harris, Graham & Corrsin (1977) and Sjögren & Johansson (1994), with the obvious consequence that one can only determine the sum of the rapid and the slow parts. The theoretical description of the kinematics of homogeneous axisymmetric turbulence by Lindborg (1995) provides new exact analytical expressions for the pressure–strain correlations as integrals over various measurable two-point velocity correlations, i.e. the solution of the Poisson equation for the pressure–strain correlation. This newly developed theoretical work opens up the possibility of separately measuring the different parts of the pressure–strain tensor in a flow with finite strain.

In this investigation the slow pressure–strain and the rapid pressure–strain have been measured in the presence of finite strain in the contraction in a wind tunnel. These are the first measurements presented in the literature to this date in which the different parts of the pressure–strain have been obtained separately. The slow pressure–strain was also determined from two-point third-order velocity moments in the relaxation towards isotropy downstream of the contraction. Also, the dissipation rate anisotropy has a direct influence on the evolution of Reynolds stress anisotropy, and was determined directly from measurements both in the strained and the relaxation phases.

In §2 we will first analyse the return-to-isotropy process without the restriction of axisymmetry. The need for nonlinear models is here demonstrated. The Lindborg (1995) formulation for the kinematics of axisymmetric turbulence is reviewed in §3, with emphasis on the integral description of the pressure–strain terms. The modelling approach, within the context of Reynolds stress closures, for the redistribution terms is briefly discussed in §4. The experimental procedure and its validations are described in §5, and the results are given in §6, followed by some concluding remarks in §7.

2. General formulation of return to isotropy

In a decaying, anisotropic, homogeneous turbulence field without mean velocity gradients the production terms, $(\mathcal{P}, \mathcal{P}^\varepsilon, \mathcal{P}_{ij}^{(a)})$, the diffusion related terms, $(J_k, J_k^\varepsilon, \text{Diff}_{ij}^{(a)})$, and the rapid pressure–strain, $\Pi_{ij}^{(r)}$, vanish. For this situation interest will be focused on the slow pressure–strain correlation, $\Pi_{ij}^{(s)}$, and the dissipation rate anisotropy, e_{ij} . The governing Reynolds stress transport (RST) equations for anisotropic turbulence relaxing towards isotropy in a homogeneous turbulent field are

$$\frac{da_{ij}}{dt} = \frac{\varepsilon}{K} \left(\frac{\Pi_{ij}^{(s)}}{\varepsilon} - e_{ij} + a_{ij} \right), \quad (2.1)$$

$$\frac{dK}{dt} = -\varepsilon, \quad (2.2)$$

$$\frac{d\varepsilon}{dt} = T\varepsilon - D\varepsilon. \quad (2.3)$$

From equation (2.2) one can see that the natural timescale for the decay of turbulence kinetic energy is $\tau_d = K/\varepsilon$,

$$\frac{1}{\tau_d} = -\frac{1}{K} \frac{dK}{dt} = \frac{\varepsilon}{K}. \quad (2.4)$$

Following the work by Lumley & Newman (1977), the natural way to close the above set of equations, within the RST context, is to model the terms on the right-hand side as functions of a_{ij} , its invariants, II_a, III_a , and the turbulent Reynolds number, Re_T :

$$II_a = a_{ik}a_{ki}, \quad III_a = a_{ij}a_{jk}a_{ki}, \quad Re_T = \frac{4K^2}{v\varepsilon}. \quad (2.5)$$

For modelling purposes it is also convenient to introduce

$$F = 1 - \frac{9}{8}(II_a - III_a), \quad A = 6^{1/2} \frac{III_a}{II_a^{3/2}}, \quad (2.6)$$

where we can see that $0 \leq F \leq 1$ and $-1 \leq A \leq 1$. The quantity $(1 - F)$ is a measure of the ‘degree of two-componentality’ being unity in the two-component limit and A is the ‘degree of axisymmetry’. The most general expression for what is often referred to as the ‘return-to-isotropy’ tensor, ϕ_{ij} , can, using the theory of invariants, be written

$$-\phi_{ij} = \frac{\Pi_{ij}^{(s)}}{\varepsilon} - e_{ij} = \gamma_1 a_{ij} + \gamma_2 (a_{ik}a_{kj} - \frac{1}{3}II_a \delta_{ij}), \quad (2.7)$$

where $\gamma_1 = \gamma_1(II_a, III_a, Re_T)$ and $\gamma_2 = \gamma_2(II_a, III_a, Re_T)$. Correspondingly, assuming that τ_d is characteristic also for the decay of the total dissipation rate, the right-hand side of equation (2.3) is given by

$$T\varepsilon - D\varepsilon = -\psi \frac{\varepsilon^2}{K}, \quad (2.8)$$

where $\psi = \psi(II_a, III_a, Re_T)$. The different nature of $T\varepsilon$ and $D\varepsilon$ could suggest separate modelling of them, as discussed by Cambon, Jacquin & Lubrano (1992). We have now reduced the problem of the return to isotropy in homogeneous turbulence to the determination of the form of three functions of the independent invariants of the anisotropy tensor and the Reynolds number. One of the limitations of using a second-order closure, i.e. using algebraic models, is that they automatically give the

same principal axes of the modelled tensor as those of the tensor it is modelled by. This is not generally true for shear flows.

To separate different physical aspects in the process of intercomponent transfer, i.e. those arising from pressure fluctuations and those related to dissipative effects, one normally splits equation (2.7) into two parts

$$e_{ij} = \alpha_1 a_{ij} + \alpha_2 (a_{ik} a_{kj} - \frac{1}{3} II_a \delta_{ij}), \quad (2.9)$$

$$\frac{\Pi_{ij}^{(s)}}{\varepsilon} = \beta_1 a_{ij} + \beta_2 (a_{ik} a_{kj} - \frac{1}{3} II_a \delta_{ij}), \quad (2.10)$$

$$\gamma_1 = \beta_1 - \alpha_1, \quad \gamma_2 = \beta_2 - \alpha_2. \quad (2.11)$$

This split was used neither by Choi (1983) nor Le Penven *et al.* (1985) since dissipation rate anisotropy and the slow pressure-strain correlation are extremely difficult to measure separately and essentially no data from such experiments have yet been reported in the literature.

In order to examine the return-to-isotropy process without any knowledge of the different parts of the return-to-isotropy tensor one can use the transport equations for the Reynolds stress anisotropy invariants. Using the assumption (2.7) these equations can be written

$$\tau_d \frac{dII_a}{dt} = 2((\gamma_1 + 1)II_a + \gamma_2 III_a), \quad (2.12)$$

$$\tau_d \frac{dIII_a}{dt} = 3((\gamma_1 + 1)III_a + \gamma_2 \frac{1}{6} II_a^2). \quad (2.13)$$

This set of equations provides implicit relations between the unknown functions γ_1, γ_2 (and thereby also the return-to-isotropy tensor ϕ_{ij}) and the Reynolds stress anisotropy invariants in decaying anisotropic homogeneous turbulence. Apart from the decay timescale τ_d , one can also define two timescales for the return to isotropy:

$$\frac{1}{\tau_{r_1}} = -\frac{1}{2II_a} \frac{dII_a}{dt}, \quad \frac{1}{\tau_{r_2}} = -\frac{1}{3III_a} \frac{dIII_a}{dt}, \quad (2.14)$$

giving the two ratios

$$r_1 = \frac{\tau_d}{\tau_{r_1}} = -\left((\gamma_1 + 1) + \gamma_2 \frac{III_a}{II_a}\right) = \frac{1}{2} \frac{d(\log II_a)}{d(\log K)}, \quad (2.15)$$

$$r_2 = \frac{\tau_d}{\tau_{r_2}} = -\left((\gamma_1 + 1) + \gamma_2 \frac{II_a^2}{6III_a}\right) = \frac{1}{3} \frac{d(\log |III_a|)}{d(\log K)}, \quad (2.16)$$

which can be determined as the slopes of the curves $\log(II_a)$, $\log(|III_a|)$ versus $\log(K)$, (see figure 1a). Solving this ($II_a^3 \neq 6III_a^2$) linear system for γ_1 and γ_2 yields

$$\gamma_1 = -1 - \frac{r_1 II_a^3 - r_2 6III_a^2}{II_a^3 - 6III_a^2} = -1 - \frac{r_1 - r_2 A^2}{1 - A^2}, \quad (2.17)$$

$$\gamma_2 = \frac{6II_a III_a (r_1 - r_2)}{II_a^3 - 6III_a^2} = \frac{6III_a}{II_a^2} \frac{r_1 - r_2}{1 - A^2}. \quad (2.18)$$

We can now give some interpretations of the functions γ_1 and γ_2 . First we note that if the different return timescales are equal ($\tau_{r_2} = \tau_{r_1}$ or $r_2 = r_1$), the need for a quadratic tensor term vanishes. Hence, we may then take $\gamma_1 = -1 - r_1$, $\gamma_2 = 0$, where r_1 still is

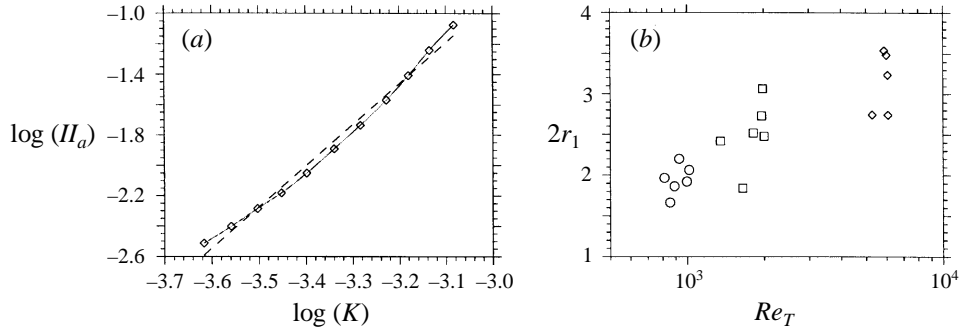


FIGURE 1. (a) $\log(II_a)$ versus $\log(K)$ from experimental data ($Re_T = 2000$) of axisymmetric anisotropic turbulence relaxing towards isotropy. Solid line represents a spline fit to the data points, dashed line represents linear regression. (b) The timescale ratio r_1 from different experiments determined by linear regression as in (a) versus the turbulence Reynolds numbers. See table 1 for symbols.

a function of II_a and III_a . Note that equations (2.15)–(2.18), based on the assumption (2.7), hold for any type of homogeneous anisotropic turbulence relaxing towards isotropy. For the case where $II_a^3 = 6III_a^2$, i.e. axisymmetric turbulence we have

$$r_1 = r_2 = - \left((\gamma_1 + 1) + \text{sign}(III_a)\gamma_2 \left(\frac{1}{6}II_a \right)^{1/2} \right). \quad (2.19)$$

Since the timescale ratios are necessarily equal in axisymmetric turbulence one cannot separate the different roles of the linear and the quadratic tensor terms in this case. The new experimental results for axisymmetric turbulence will be discussed in the following sections. As a preamble it is, however, interesting to illustrate the above analysis by some experimental observations of axisymmetric turbulence.

In figure 1(a) we can see the return-to-isotropy process in terms of $\log(II_a)$ versus $\log(K)$ from data taken in the test section of the wind tunnel. The linear regression (dashed line) in figure 1(a) deviates significantly from the experimental results and indicates that the functions (γ_1, γ_2) cannot be constants, but must depend on the invariants of a_{ij} . Figure 1(b) shows the timescale ratio r_1 taken from different experiments, determined by linear regression (as in figure 1a), versus the turbulence Reynolds numbers. It is seen that γ_1 and γ_2 are functions of the turbulence Reynolds number. Hence, these results clearly demonstrate the need for complex nonlinear modelling, including turbulence Reynolds number dependence, for the return-to-isotropy tensor.

In the final period of decay (Batchelor 1953, p. 92), where $Re_T \rightarrow 0$, the momentum equation may be written as

$$\frac{d\overline{u_i u_j}}{dt} = -\varepsilon_{ij}, \quad \text{or} \quad \tau_d \frac{da_{ij}}{dt} = a_{ij} - e_{ij}. \quad (2.20)$$

This state corresponds to very small Reynolds number, and consequently negligible influence of inertial terms. Hence, the interchange of energy between the components is only due to viscous effects. Equation (2.20) implies that for $Re_T \rightarrow 0$

$$\gamma_1 \rightarrow -\alpha_1, \quad \gamma_2 \rightarrow -\alpha_2. \quad (2.21)$$

From an experimental point of view axisymmetric turbulence is a convenient and important flow case to examine, since methods exist for determining all of the significant quantities involved in the problem, including the pressure-strain rate,

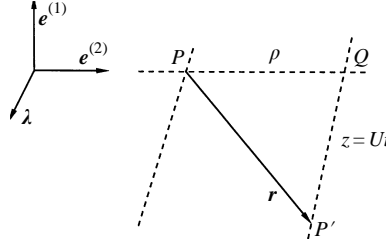


FIGURE 2. The double X-probe configuration. One probe is located at an arbitrary point P in the homogeneous field and the other probe is located at point Q . The point P' downstream of Q is reached by use of Taylor's hypothesis.

Lindborg (1995). From an invariant modelling point of view, however, a more general anisotropic state would be preferable, in order to enable separation of the effects arising from the linear and the nonlinear parts of the algebraic model.

3. Axisymmetric turbulence

In axisymmetry there is one and only one vector, λ , determining the overall symmetry of the physical state. In axisymmetric turbulence that satisfies reflectional symmetry, i.e. insensitivity to a change $\lambda \rightarrow -\lambda$, one needs four scalar functions to completely describe the two-point second-order velocity correlation tensor, Batchelor (1953, 1946). These are in turn related through two continuity relations, see also Chandrasekhar (1950). To describe the two-point third-order velocity correlation tensor completely one needs ten scalar functions, Lindborg (1995). From the separation vector, \mathbf{r} , and the vector, λ , defining the axis of symmetry one may construct the two orthogonal unit vectors

$$\mathbf{e}^{(1)} = \frac{1}{\rho} \lambda \times \mathbf{r}, \quad \mathbf{e}^{(2)} = \mathbf{e}^{(1)} \times \lambda, \quad (3.1)$$

with the result that the separation vector is given by $\mathbf{r} = z\lambda + \rho\mathbf{e}^{(2)}$. The formalism based on this choice of coordinate system bears significant similarities with the 'Craya-Herring' type of description in spectral space (see Cambon *et al.* 1992).

Following Lindborg (1995) we can now express the two-point second-order correlation tensor as

$$R_{ij}(\mathbf{r}) = \lambda_i \lambda_j R_1 + e_i^{(2)} e_j^{(2)} R_2 + e_i^{(1)} e_j^{(1)} R_3 + (\lambda_i e_j^{(2)} + \lambda_j e_i^{(2)}) R_4.$$

Here, each scalar function depends on the scalars $\rho = |\lambda \times \mathbf{r}|$ and $z = \mathbf{r} \cdot \lambda$. The advantage of this approach is that the scalar functions represent correlations which are naturally suggested by the cylindrical geometry. If the fluctuating velocity vector is taken to be $u\lambda + v\mathbf{e}^{(2)} + w\mathbf{e}^{(1)}$ we may interpret u as the axial, v as the radial and w as the azimuthal velocity components in a local cylindrical coordinate system at an arbitrary point P in the homogeneous field. The scalar functions are then

$$R_1 = \overline{uu'}, \quad R_2 = \overline{vv'}, \quad R_3 = \overline{ww'}, \quad R_4 = \overline{uv'} \quad (3.2)$$

where the primed velocities are taken at a point P' with separation vector \mathbf{r} relative to P . With two probes mounted on a device that can vary the distance between the probes perpendicular to the mean flow (see figure 2), and use of Taylor's hypothesis, the whole (ρ, z) -plane can be covered and the different scalar functions can be measured.

For the two-point third-order correlation tensor one has, Lindborg (1995),

$$\begin{aligned}
M_{ikj}(\mathbf{r}) = & \lambda_i \lambda_k \lambda_j M_1 + e_i^{(2)} e_k^{(2)} \lambda_j M_2 + e_i^{(1)} e_k^{(1)} \lambda_j M_3 \\
& + \lambda_i \lambda_k e_j^{(2)} M_4 + e_i^{(2)} e_k^{(2)} e_j^{(2)} M_5 + e_i^{(1)} e_k^{(1)} e_j^{(2)} M_6 \\
& + (\lambda_i e_k^{(2)} + \lambda_k e_i^{(2)}) \lambda_j M_7 + (\lambda_i e_k^{(2)} + \lambda_k e_i^{(2)}) e_j^{(2)} M_8 \\
& + (\lambda_i e_k^{(1)} + \lambda_k e_i^{(1)}) e_j^{(1)} M_9 + (e_i^{(2)} e_k^{(1)} + e_k^{(2)} e_i^{(1)}) e_j^{(1)} M_{10},
\end{aligned} \tag{3.3}$$

where

$$\left. \begin{aligned}
M_1 &= \overline{uuu'}, & M_2 &= \overline{vvv'}, & M_3 &= \overline{www'}, \\
M_4 &= \overline{uuv'}, & M_5 &= \overline{vvv'}, & M_6 &= \overline{wwv'}, \\
M_7 &= \overline{uvu'}, & M_8 &= \overline{uvv'}, & M_9 &= \overline{uww'}, & M_{10} &= \overline{vww'}.
\end{aligned} \right\} \tag{3.4}$$

For homogeneous flows the rapid pressure–strain rate can be written in terms of a fourth-rank tensor

$$\Pi_{ij}^{(r)} = 4K \frac{\partial U_p}{\partial x_q} (\mathcal{M}_{iqpj} + \mathcal{M}_{jqpi}) \tag{3.5}$$

in which

$$\mathcal{M}_{ijpq} = -\frac{1}{8\pi K} \int \frac{\partial^2 R_{ij}}{\partial r_p \partial r_q} \frac{dV}{|\mathbf{r}|} = \frac{1}{2K} \int \frac{\kappa_p \kappa_q}{\kappa_m \kappa_m} \Phi_{ij} d^3 \kappa \tag{3.6}$$

where κ is the wavenumber and Φ_{ij} is the spectrum tensor. The expressions (3.5), (3.6) come from the formal solution of the Poisson equation for the pressure field. For further details and discussion of the \mathcal{M} -tensor see Johansson & Hallbäck (1994).

The slow pressure–strain rate

$$\Pi_{ij}^{(s)} = \frac{1}{4\pi} (\delta_{mi} \delta_{nj} + \delta_{mj} \delta_{ni}) \int \frac{\partial^3 \overline{u_m u_p' u_q'}}{\partial r_n \partial r_p \partial r_q} \frac{dV}{|\mathbf{r}|} \tag{3.7}$$

can, correspondingly, be expressed with the M_{ikj} tensor.

With the aid of the scalar functions in (3.2) and (3.4) we may (Lindborg 1995) express the two parts of the pressure–strain correlation after partial integration as

$$\Pi_{11}^{(r)} = \sigma \int_0^\infty \int_0^\infty 18\rho^2 z r^{-5} R_4 dz d\rho = 12K \sigma \mathcal{M}_{1111}, \tag{3.8}$$

$$\begin{aligned}
\Pi_{11}^{(s)} = & \int_0^\infty \int_0^\infty [6\rho z r^{-7} (2z^2 - 3\rho^2) (M_1 - M_2) \\
& + 6\rho z r^{-5} (M_2 - M_3) + 6\rho^2 r^{-7} (4z^2 - \rho^2) M_7] dz d\rho,
\end{aligned} \tag{3.9}$$

where the axisymmetric straining parameter is denoted by $\sigma = \partial U / \partial x$. With two X-probes separated on a line perpendicular to the mean flow one can thus measure these functions (using Taylor's hypothesis in the symmetry direction) and thereby also the pressure–strain term. One may note that the \mathcal{M}_{1111} component can be measured both in the presence and the absence of mean strain.

4. Modelling

Some aspects of the modelling of the terms affecting the intercomponent Reynolds stress redistribution are briefly discussed below, as a basis for the evaluation of the

experimental results. More detailed discussion of these can be found in e.g. Sjögren & Johansson (1997) and Hallböck *et al.* (1995).

4.1. Dissipation rate anisotropy

The most common way of modelling the dissipation rate anisotropy tensor e_{ij} is simply to put $e_{ij} = 0$, which is based on the assumption that the scales in which dissipation occurs are isotropic. Experimental results show that this is often not a good approximation for moderate Reynolds number. In situations near the two-component limit it obviously gives a poor prediction and may cause unphysical results. Schumann (1977) pointed out that if the energy of one of the fluctuating velocity components vanishes, the time derivative of that component must also vanish in order to avoid subsequent negative values of the corresponding normal Reynolds stress component. Hallböck, Groth & Johansson (1990), used that requirement to derive a third-order realizable model for the dissipation rate anisotropy

$$e_{ij} = [1 + \alpha(\frac{1}{2}\Pi_a - \frac{2}{3})]a_{ij} - \alpha(a_{ik}a_{kj} - \frac{1}{3}\Pi_a\delta_{ij}). \quad (4.1)$$

The model parameter α was determined from rapid distortion theory to be $3/4$ in order to get correct initial behaviour of the dissipation rate anisotropies in the case of suddenly distorted isotropic turbulence.

At a solid wall the two-component limit is approached in such a way that not only $e_{ij}n_in_j = a_{ij}n_in_j$, where n_i is the wall-normal vector, but also $e_{ij} = a_{ij}$. Hence, the limiting value of the whole dissipation rate anisotropy tensor is identical to a_{ij} . A third-order model cannot capture this behaviour. Instead, a fifth-order model may be derived

$$e_{ij} = (1 + a'_1F)a_{ij} + a_2F(a_{ik}a_{kj} - \frac{1}{3}\Pi_a\delta_{ij}) \quad (4.2)$$

where F is a ‘two-componentality’ parameter (see (2.6)) and $a'_1 = -1/2$ in order to ensure a correct initial response to a sudden rapid distortion. The remaining model parameter a_2 must be calibrated against some chosen flow situation.

The model parameters may also be allowed to depend on the turbulence Reynolds number but not on the a_{ij} invariants. Such a model was derived and discussed in Sjögren & Johansson (1997) and will be compared below with experimental data in axisymmetric turbulence, where the dissipation rate anisotropy has been directly measured.

4.2. Slow pressure–strain

The simplest model of the slow pressure–strain rate,

$$\Pi_{ij}^{(s)} = \frac{p^{(s)}}{\rho} \left(\frac{\partial u_i}{\partial x_j} + \frac{\partial u_j}{\partial x_i} \right), \quad (4.3)$$

is the linear Rotta (1951) model

$$\frac{\Pi_{ij}^{(s)}}{\varepsilon} = -C_1 a_{ij}, \quad (4.4)$$

where C_1 is known as the ‘Rotta constant’, normally assigned a value of about 1.5 to 1.8. A strong dependence of C_1 on the turbulence Reynolds number was found in direct numerical simulations by Hallböck *et al.* (1993), and was recently confirmed and extended by LES to higher Reynolds number by Alvelius, Hallböck & Johansson (1997). In the simulations of Hallböck *et al.* (1993) isotropic turbulence was subjected

to an axisymmetric mean distortion from which it was allowed to relax towards isotropy, with Re_T in the relaxation phases in the range 10 to 400. Hallbäck *et al.* (1993) proposed a model for this Reynolds number variation, based on Rotta's original proposal, in which

$$C_1 = C_{1\infty} \left(\left[2 \frac{Re_T}{R_b} + \left(\frac{Re_T}{R_b} \right)^2 \right]^{1/2} - \frac{Re_T}{R_b} \right) = C_{1\infty} f(Re_T) \quad (4.5)$$

with $R_b = 1308$ and $C_{1\infty} = 2.58$. The Rotta constant, C_1 , is predicted by this model to approach $C_{1\infty} = 2.58$ as $Re_T \rightarrow \infty$. A lower limiting value was obtained from the LES of Alvelius *et al.* (1997). In order to capture the variation of $\Pi_{ij}^{(s)}$ with the 'amplitude' of the anisotropy it was shown in Sjögren & Johansson (1997) that a fifth-order model is needed. The general form is given by basic tensor theory (see e.g. Lumley & Newman 1977) and reads

$$\frac{\Pi_{ij}^{(s)}}{\varepsilon} = f(Re_T) [\beta_1 a_{ij} + \beta_2 (a_{ik} a_{kj} - \frac{1}{3} II_a \delta_{ij})] \quad (4.6)$$

We have here lumped the Reynolds number dependence into the single function $f(Re_T)$ given by equation (4.5). The fifth-order algebraic slow pressure-strain model of Sjögren & Johansson (1997) is specified by

$$\beta_1 = c_1 F + \left(\frac{9}{8} c_1 + c_3 \right) \left(\frac{8}{9} (F - 1) + 2 II_a - II_a^2 \right), \quad (4.7)$$

$$\beta_2 = c_2 F + \left(\frac{9}{8} c_1 + c_3 \right) \left(\frac{1}{2} II_a + \frac{3}{2} III_a \right), \quad (4.8)$$

The values of c_1 , c_2 and c_3 were determined by Sjögren & Johansson (1997) as -2.4 , 2.2 and 1.2 respectively, from calibration against DNS data.

4.3. Rapid pressure-strain

The rapid part of the pressure-strain rate can in homogeneous cases be expressed with the aid of the fourth rank-tensor \mathcal{M} -tensor (see (3.5) and (3.6)). This starting point for the modelling within Reynolds stress closures is normally assumed to be valid also for moderately inhomogeneous situations. The natural approach is then to assume the \mathcal{M} -tensor to be expressible in the Reynolds stress anisotropy tensor. Requirements of physical realizability necessitate the use of models that are nonlinear in a_{ij} . Such models were discussed in detail in Johansson & Hallbäck (1994) (extended in Sjögren & Johansson 1997) and further analysed in e.g. Ristorcelli, Lumley & Abid (1996).

For instance, the model of Johansson & Hallbäck (1994) is of fourth order in a_{ij} and in that paper was tested in a variety of homogeneous flows. Models of this kind have in several studies been shown to give superior predictive capability in comparison with linear models (see also Speziale, Sarkar & Gatski 1991). Still, for all models based on the assumption of describing the \mathcal{M} -tensor in a_{ij} there are rather severe limitations in describing effects of strong rotation, as discussed by e.g. Kassinos & Reynolds (1994), Cambon, Mansour & Godefred (1997) and Johansson (1995). This has also been nicely demonstrated experimentally and through EDQNM-calculations by Leuchter & Dupeuble (1993) and Leuchter & Cambon (1997).

4.4. The modelling of return-to-isotropy in axisymmetric turbulence

It has been observed from numerical and physical experiments (Lee & Reynolds 1985 and Choi 1983) that the return to isotropy is slower after an axisymmetric

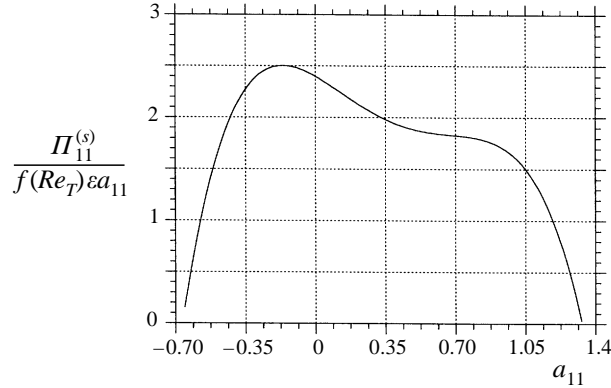


FIGURE 3. The effective Rotta constant in axisymmetric turbulence versus Reynolds stress anisotropy a_{11} for the fifth-order model.

expansion than after a contraction. In the expansion case the third invariant of the stress anisotropy tensor is positive. Hence, with $\lambda_i = \delta_{i1}$ the anisotropy component a_{11} is here positive, and the kinetic energy tends to be concentrated in one component. In the contraction case on the other hand, a_{11} and III_a are negative, and for large degrees of anisotropy we approach a two-component limit.

The models described above inherently give different rates of return depending on the sign of a_{11} . If we choose $a_2 = 0$ in the dissipation model (as primarily discussed in Sjögren & Johansson 1997), this effect enters mainly through the slow pressure-strain model. In axisymmetric turbulence the fifth-order model can be written

$$\frac{\Pi_{11}^{(s)}}{f(Re_T)\epsilon a_{11}} = \beta_1 + \frac{1}{2}\beta_2 a_{11}. \quad (4.9)$$

This form can be interpreted as the effective asymptotic Rotta constant, and is shown in figure 3. We note the asymmetric behaviour around the isotropic state with significantly lower values for small positive anisotropies than for negative ones. This is at least in qualitative agreement with observed behaviour.

The initial relaxation phase after an expansion exhibits some complex features (Lee & Reynolds 1985). The Reynolds stress anisotropy may in some cases even increase in the initial relaxation. Such a feature is not really possible to capture with the ‘classical’ Reynolds stress models discussed in the present paper. The lag between the development of second- and third-order moments could here possibly be a key factor. If so, a reasonable prediction of this phenomenon would require modelling of transport equations for triple moments.

5. Experimental setup

5.1. The wind tunnel

The experiments have been carried out in the MTL low-turbulence, low-speed wind-tunnel at KTH, see Johansson (1992). The wind tunnel (figure 4) has a 4 m long contraction, with an area ratio of 9, followed by a 7 m long test section. The rectangular cross-section of the test section is 0.8 m \times 1.2 m. The variation of the mean velocity along the centreline of the test section is less than 0.5%. This means that effects due to mean distortion of the turbulence field in the test section are negligible. The uniformity of the mean flow in the cross-stream plane is within 0.1%.

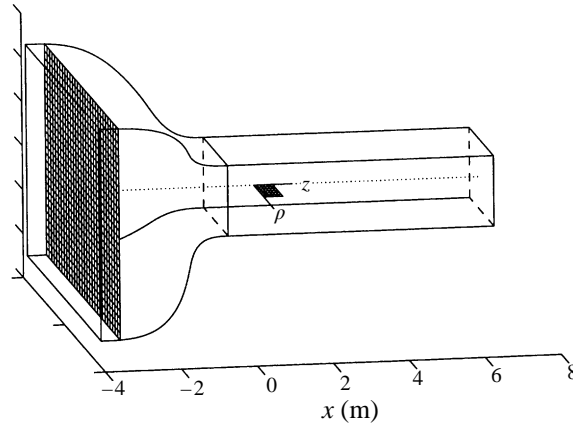


FIGURE 4. Wind-tunnel contraction and test section. Test section starts at $x = 0$ m and ends at $x = 7$ m. Cross section: 0.8×1.2 m. Contraction area ratio: 9. Grid location: $x = -6$ m, $x = -4.5$ m and $x = -3.5$ m for studies of highly anisotropic turbulence, $x = -1$ m for studies of isotropic turbulence. The shape of the contraction is given by $A(\sinh(Bx/L) - Bx/L)$ for $-4 \leq x \leq -2.8$ m and $1 - C(\sinh(D(1 - x/L)) - D(1 - x/L))$ for $-2.8 \leq x \leq 0$ m, where $A = 0.20582$, $B = 3.52918$, $C = 0.08819$, $D = 8.23523$ and $L = 4$.

Turbulence was generated by a monoplane square rod grid with 10 cm mesh width and a solidity of 36% (rod width = 2 cm) positioned at the beginning of the contraction. In the contraction the turbulence is strongly distorted by the accelerating mean flow producing a turbulence state at the beginning of the test section that is highly anisotropic with relative turbulence levels around 1%. In the test section the turbulence is allowed to relax towards isotropy in the absence of any mean strain. The turbulence Reynolds number $Re_T \equiv 4K^2/\nu\varepsilon$ is typically about 5000 in the experiments.

5.2. Data acquisition

A double X-probe configuration was used for all the velocity measurements. The hot-wire X-probes had $2.5 \mu\text{m}$ platinum wire sensors and a measurement volume of $(0.75 \text{ mm})^3$. A Macintosh Quadra 950 running LabVIEW controlled a five-axis traversing system, which made it possible to fully automatically carry out an angular calibration procedure of two X-probes simultaneously. Third-order polynomials were fitted to the calibration data, divided into about seven different mean velocities and angles, over a velocity range of $\pm 5\%$ of the mean speed used. The air temperature was maintained constant (and uniform) within $\pm 0.1^\circ\text{C}$ during calibration and measurement.

A hot-wire anemometer from AA-systems together with a 4-channel 12 bit AD-converter was used to collect the data from the two X-probes. The probes were traversed and sampled at about 30 separations and five downstream locations. At each position $4 \times 1024 \times 500$ samples were taken at a sampling rate corresponding to the inverse of the energy decay timescale. This gave approximately 650 Mb of data from each experiment which were subsequently saved on a recordable compact disc (CD-R) for later post processing.

5.3. Probe configuration

A hot-wire X-probe can measure two of the three orthogonal velocity components present in a turbulent field. Consequently there are three different principal ways of

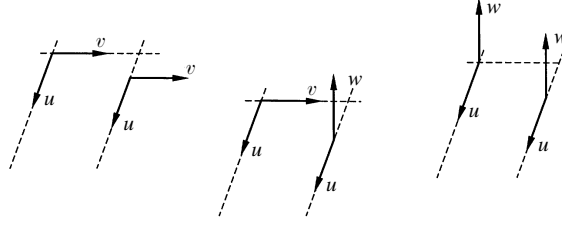


FIGURE 5. The VV-, VW- and WW-configurations.

mounting the two probes in axisymmetric turbulence (figure 5). The configuration in which the axial, u , and the radial, v , velocity components are measured at both points will be referred to as a VV-configuration. With a so-called VW-configuration u and v are measured at one point, while at the other point u and the azimuthal, w , velocity are measured. This is achieved by rotating one probe 90° after calibration. The probe-holding device allowed the distance between the probes to be varied during experiments.

5.4. Measurement techniques

For measurements in the test section the measuring device was mounted on a 1 m long sting connected to a traversing tower that enables measurements in the region $0 \leq x \leq 5$ m of the test section. The traversing range normal to the mean flow is 0.5 m.

For measurement in the contraction the probe holding device was mounted on a 5 m long sting, especially manufactured for this particular experiment. The sting is made from high E-module carbon fibre and with a construction to maximize stiffness to reduce vibrations. The short sting was mounted at the end of this long sting, which made it possible to measure up to 3.5 m upstream of the test section (i.e. to $x = -3.5$ m).

A Prandtl tube was mounted beside the measuring device, which was used in the calibration procedure for measurement in the contraction. In this case the hot wires were calibrated by keeping the mean velocity constant in the test section and exposing the probes to different velocities by traversing the measuring device through the contraction.

5.5. Experimental validation

By mounting the monoplane grid 1 m upstream of the test section one can produce nearly isotropic turbulence. This is somewhat analogous to the technique of Comte-Bellot & Corrsin (1966) to produce isotropic turbulence, in their case by a contraction further downstream of the grid.

In the isotropic case the two-point third-order velocity correlation tensor, usually referred to as the triple correlation tensor, can be written, Hinze (1975),

$$M_{ikj} = u_{rms}^3 \left[\frac{1}{2r^3} \left(k - r \frac{dk}{dr} \right) r_i r_k r_j + \frac{1}{4r} \left(2k + r \frac{dk}{dr} \right) (r_i \delta_{kj} + r_k \delta_{ij}) - \frac{k}{2r} r_j \delta_{ik} \right]. \quad (5.1)$$

Here $k(r)$ is the triple correlation between three velocity components all oriented in the direction of r . This quantity can easily be measured with a single hot wire and has been the subject of many experimental investigations since the early work of Simmons & Salter (1934). The function $k(r)$ is shown in figure 6; the symbols represent data from experiments in the MTL wind tunnel in nearly isotropic turbulence and the

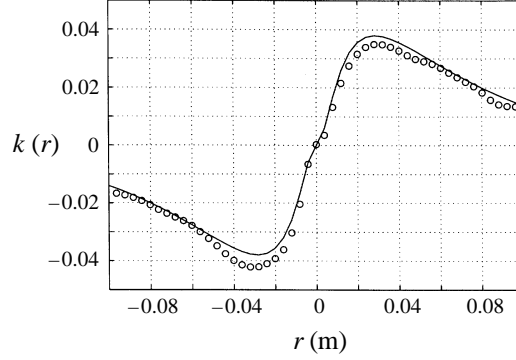


FIGURE 6. Triple correlation function $k(r)$ in nearly isotropic turbulence ($Re_T = 2000$). Symbols: experimental data from the MTL wind tunnel. Solid line: analytical approximation given by equation (5.2), with $a = 1.17 \times 10^6 \text{ m}^{-3}$, $b = 3.47 \times 10^8 \text{ m}^{-5}$ and $c = 40.2$ (integral scale $\mathcal{L}_{uz} = 0.023 \text{ m}$).

solid line is the analytical expression

$$k(r) = (ar^3 + br^5) \exp(-c|r|^{1/2}) \quad (5.2)$$

which is a curve fit that captures the general behaviour of $k(r)$.

Since isotropy is a special case of axisymmetry one can use the equations (3.3) and (5.1) to express the M -functions in terms of $k(r)$. For example the functions M_1 , M_2 and M_3 in isotropy with $r = (z^2 + \rho^2)^{1/2}$ read

$$\left. \begin{aligned} M_1(\rho, z) &= \frac{u_{rms}^3}{2} \left[\left(k - r \frac{dk}{dr} \right) \frac{z^3}{r^3} + \left(k + r \frac{dk}{dr} \right) \frac{z}{r} \right], \\ M_2(\rho, z) &= \frac{u_{rms}^3}{2} \left[\left(k - r \frac{dk}{dr} \right) \frac{z\rho^2}{r^3} - k \frac{z}{r} \right], \\ M_3(\rho, z) &= \frac{u_{rms}^3}{2} k \frac{z}{r}. \end{aligned} \right\} \quad (5.3)$$

Figure 7 shows the behaviour of some of the different M -functions in isotropic turbulence calculated from measurement with one single hot wire. The agreement with the M -functions in figure 8 measured directly with two hot-wire X-probes is very good, considering the difficulty, time and effort involved in the latter method. These two figures serve as a validation of the experimental techniques and the assumptions involved in determining the correlations of interest in axisymmetric turbulence and also of the fact that isotropic turbulence can be produced by use of a monoplane grid.

5.6. Measurable quantities

With the probes configured in the same way as they were calibrated, i.e. in a VV-configuration, it is possible to fully determine R_1 and R_2 in equation (3.2). From these functions one can derive the single-point statistical quantities

$$\overline{u^2} = R_1(0, 0), \quad \overline{v^2} = R_2(0, 0), \quad (5.4)$$

$$\left. \begin{aligned} \lambda_{uz}^2 &= \lim_{z \rightarrow 0} \frac{z^2}{1 - (R_1(z, 0)/R_1(0, 0))}, & \lambda_{vz}^2 &= \lim_{z \rightarrow 0} \frac{z^2}{1 - (R_2(z, 0)/R_2(0, 0))}, \\ \lambda_{u\rho}^2 &= \lim_{\rho \rightarrow 0} \frac{\rho^2}{1 - (R_1(0, \rho)/R_1(0, 0))}, & \lambda_{v\rho}^2 &= \lim_{\rho \rightarrow 0} \frac{\rho^2}{1 - (R_2(0, \rho)/R_2(0, 0))}, \end{aligned} \right\} \quad (5.5)$$

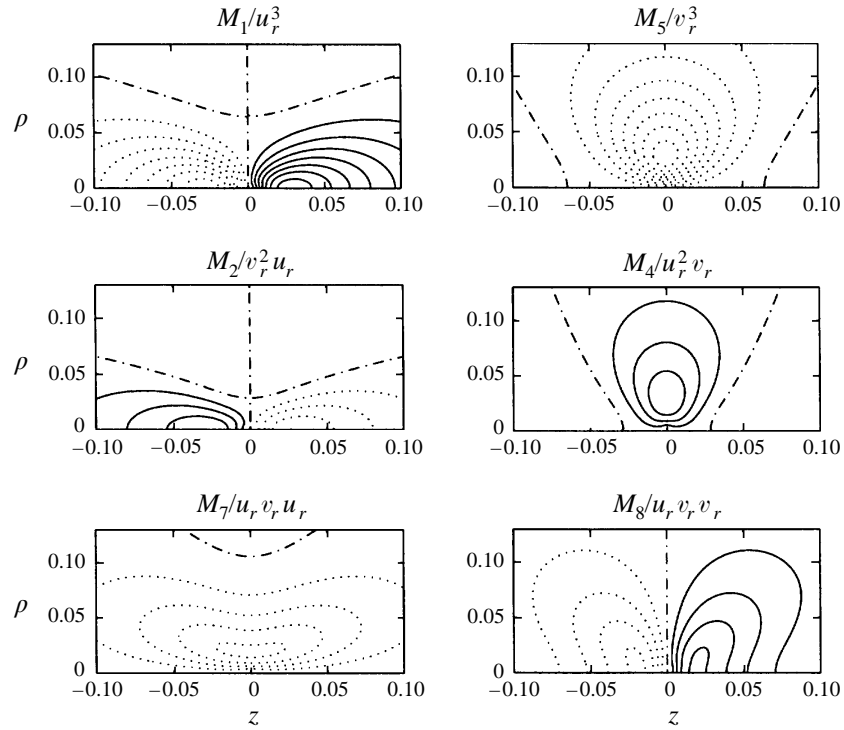


FIGURE 7. Normalized M -functions determined from $k(r)$ in nearly isotropic turbulence. (Contour increment 0.005.) $u_r = (\overline{u^2})^{1/2}$, $v_r = (\overline{v^2})^{1/2}$.

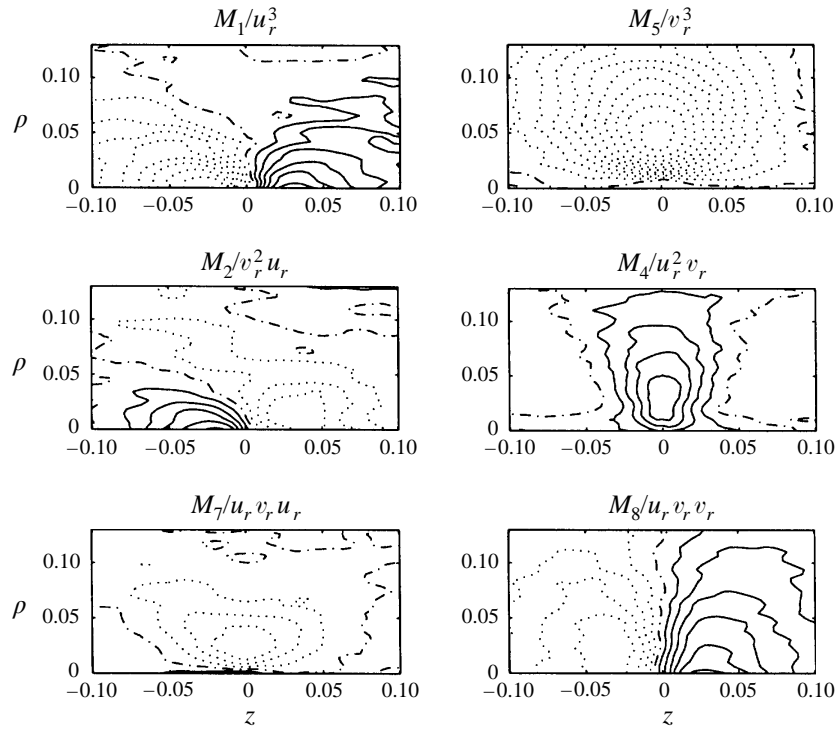


FIGURE 8. Normalized M -functions determined with two X-probes in nearly isotropic turbulence. (Contour increment 0.005.)

where the limiting values for the Taylor microscales in equation (5.5) are obtained by extrapolating data to zero separation using a polynomial fit. The method of determining the Taylor microscales and the dissipation rate anisotropy is examined and explained in detail in Hallbäck *et al.* (1993) and Sjögren & Johansson (1994). The spatial resolution is in these papers shown to be adequate in order enable an extrapolation to zero separation.

The quantities in equations (5.4) and (5.5) constitute a platform from which a great deal of the understanding of axisymmetric turbulence can be extracted. Using the various relations which can be derived for the axisymmetric case we have

$$K = \frac{1}{2}(\overline{u^2} + 2\overline{v^2}), \quad (5.6)$$

$$a_{11} = \frac{\overline{u^2}}{K} - \frac{2}{3}, \quad (5.7)$$

$$\varepsilon_{11} = 4\nu \left(\frac{\overline{u^2}}{\lambda_{uz}^2} + 2 \frac{\overline{u^2}}{\lambda_{u\rho}^2} \right), \quad (5.8)$$

$$\varepsilon_{22} = 4\nu \left(\frac{\overline{v^2}}{\lambda_{vz}^2} - \frac{\overline{u^2}}{\lambda_{uz}^2} + 4 \frac{\overline{v^2}}{\lambda_{v\rho}^2} \right), \quad (5.9)$$

$$\varepsilon^T = \frac{1}{2}(\varepsilon_{11} + 2\varepsilon_{22}), \quad (5.10)$$

where 1 is the index corresponding to the axis of symmetry. The superscript T on the dissipation signifies that the total dissipation has been evaluated by adding all the measurable velocity derivative moments obtained by a VV-configuration, using an axisymmetric relation which also was derived by George & Hussein (1991).

Another way of computing the dissipation is from the transport equation for the turbulent kinetic energy. In the test section of the wind tunnel the equations for the kinetic energy and the total dissipation rate are treated separately from the transport equation for the Reynolds stress anisotropy. This method of determining the total dissipation rate is based on a least square fit to a prescribed behaviour which is the solution to the model equations in relaxing turbulence:

$$U \frac{dK}{dx} = -\varepsilon, \quad (5.11)$$

$$U \frac{d\varepsilon}{dx} = T\varepsilon - D\varepsilon = -C_{\varepsilon 2} \frac{\varepsilon^2}{K}. \quad (5.12)$$

The solution is

$$K = (ax + b)^{1/(1-C_{\varepsilon 2})}, \quad (5.13)$$

$$\varepsilon^B = \frac{aU}{(C_{\varepsilon 2} - 1)} K^{C_{\varepsilon 2}}, \quad (5.14)$$

where only a and $C_{\varepsilon 2}$ have to be determined in order to obtain ε^B . In the fitting procedure $C_{\varepsilon 2}$ is restricted to vary between 1.4 and 2.0, since it can be shown that values outside this range give unphysical results. The ability to measure one quantity in two different ways is a powerful tool in assessing the accuracy of the experimental techniques used.

Analysis and experience, Sjögren & Johansson (1994), have shown that determination of the dissipation rate anisotropy, e_{11} , through the direct method (T) gives the

Exp.	Re_T	Grid loc. (m)	Config. a, b	$\eta_o - \eta_e$ (mm)	$\frac{L/U}{K/\varepsilon}$	No. a, b	Symbol
E1a,b	1 000	-3.5	vv,vw	1.2-1.5	0.5	6, 3	○
E2a,b	2 000	-3.5	vv,vw	0.8-0.9	0.4	6, 2	□
E3a,b	5 000	-3.5	vv,vw	0.4-0.5	0.3	7, 2	◇
E4a,b	10 000	-3.5	vv,vw	0.3-0.4	0.2	1, 1	△
E5	5 000	-6.0	vv	0.5-0.6	0.3	3	+
E6	10 000	-6.0	vv	0.4-0.5	0.2	2	×

TABLE 1. Return-to-isotropy experiments.

highest accuracy:

$$e_{11}^T = \frac{\varepsilon_{11}}{\varepsilon^T} - \frac{2}{3} = \frac{2}{1 + 2(\varepsilon_{22}/\varepsilon_{11})} - \frac{2}{3}, \quad (5.15)$$

$$e_{11}^B = \frac{\varepsilon_{11}}{\varepsilon^B} - \frac{2}{3}. \quad (5.16)$$

The measuring error that is introduced when determining the Taylor microscale is essentially cancelled when evaluating a ratio between different scales as in the anisotropy measure e_{11}^T . However, it is not evident which (ε^B or ε^T) to choose for the total dissipation.

The only way to determine the slow pressure-strain, without the new kinematic description for axisymmetric turbulence of Lindborg (1995), is from balance of the transport equation (2.1) for the Reynolds stress anisotropy tensor. Using this equation and Taylor's hypothesis we have

$$\frac{\Pi_{11}^{(s)}}{\varepsilon} = \frac{K}{\varepsilon} U \frac{da_{11}}{dx} + e_{11} - a_{11}. \quad (5.17)$$

With the VW-configuration one measures u and v at one point and u and w at the other point. The aim is that one can then determine all of the triple correlation functions M_1, M_2, M_3 and M_7 which are needed to determine the slow pressure-strain rate directly. For this situation Lindborg (1995) derived the relation (3.9) for the slow pressure-strain rate. The slow pressure-strain term can now be determined in two different ways in homogeneous axisymmetric turbulence relaxing towards isotropy: either directly from the relation (3.9) or from (5.17). The rapid part of the pressure-strain rate is computed from equation (3.8), i.e. as an integral of the second-order, two-point correlation R_4 .

In the VW-configuration it is not possible to measure the entire function $R_2 = \overline{vv'}$, but only $R_2(z, 0)$. One cannot therefore determine the Taylor microscale $\lambda_{v\rho}$ in this configuration. Hence, the quantities ε_{22} , ε^T and e_{11}^T cannot be measured in the VW-configuration.

6. Results

The different experimental runs are described in tables 1 and 2. The turbulence Reynolds number was varied from 1000 to 10 000, which was achieved by varying the mean speed in the wind tunnel.

Exp.	Re_T	Grid loc. (m)	Config. a, b	$\frac{K}{\varepsilon}$	No. a, b	Symbol
S1b	1 000	-3.5	vw	1.2	1	○
S2a,b	2 000	-3.5	vv,vw	1.0	1, 1	□
S3b	5 000	-3.5	vw	0.8	1	◇
S4a	1 000	-4.5	vv	1.2	1	●
S5a,b	2 000	-4.5	vv,vw	1.0	2, 1	■
S6a,b	5 000	-4.5	vv,vw	0.8	3, 3	◆

TABLE 2. Finite strain experiments.

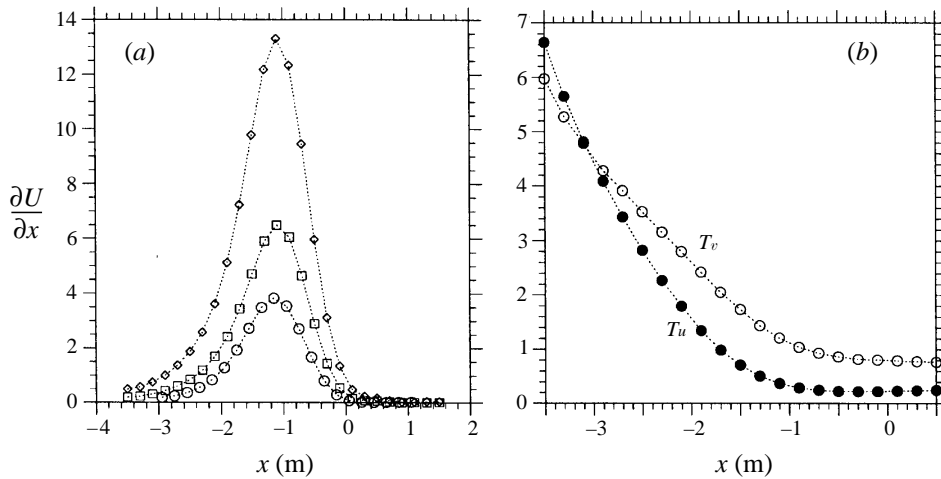


FIGURE 9. (a) Mean velocity gradient (in s^{-1}) at three different Reynolds numbers, see table 2 for symbols. (b) The turbulence level downstream of the grid. $T_u = 100u_{rms}/U$ and $T_v = 100v_{rms}/U$ at $Re_T \sim 5000$.

The largest scales in the grid-generated turbulence are essentially determined by the mesh size of the grid, which was 100 mm. The increase in the range of scales with increasing Reynolds number is given here by the decrease in the smallest scale normally referred to as the Kolmogorov scale, η , as seen from table 1. The number of eddy-turnover times is a measure of the duration of the experiment scaled with the timescale for the decay of turbulence and is given by the ratio $(L/U)/(K/\varepsilon)$, where L is the downstream distance over which the probes are traversed and U is the mean velocity. In this normalization the relaxation time may seem small, but as will be evident from the results presented below, it covers the main part of the relaxation towards isotropy. The number of repetitions of each set of measurements is also given in tables 1 and 2.

The mean velocity gradient is shown in figure 9(a) for three different Reynolds numbers. A normalization with the turbulence timescale, K/ε , yields that the maxima in figure 9(a) correspond to non-dimensional strain rates, $S^* = K/\varepsilon(2S_{ik}S_{ki})^{1/2}$, of about 2.8, 4.1 and 5.9. Hence, in parts of the contraction we should expect a behaviour close to that described by rapid distortion theory (RDT), at least for the higher Reynolds numbers.

Figure 9(b) shows the turbulence levels through the contraction and the first part of the test section. They are heavily suppressed by the high area ratio ($CR = 9$) of the contraction so that the relative levels are both below 1% after the contraction.

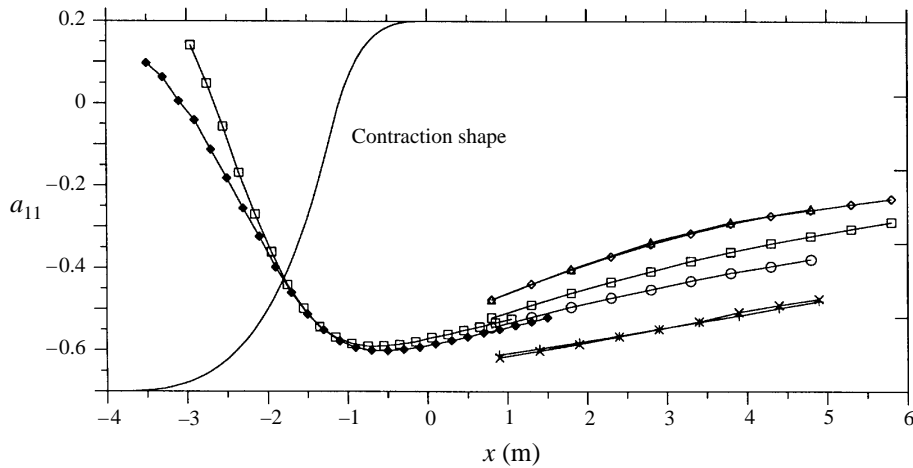


FIGURE 10. Reynolds stress anisotropy, a_{11} , versus downstream position.

The Reynolds stress anisotropy a_{11} in the contraction and in the test section is shown in figure 10. The anisotropy is slightly positive behind the grid. In the contraction the turbulence is strongly distorted by the accelerating mean flow producing a turbulence state at the beginning of the test section that is highly anisotropic. Note that $a_{33} = a_{22} = -\frac{1}{2}a_{11}$ due to axisymmetry, and that a state quite close to the two-component limit (in which $a_{11} = -2/3$) is reached in the later part of the contraction.

The measurements in the test section cover a significant part of the process of return towards isotropy. The differences in the initial values of the degree of anisotropy at the beginning of the test section is mainly due to the differences in position of the monoplane grid in the stagnation chamber. The reason for this is that the turbulence just downstream of the monoplane grid has a slightly positive anisotropy, a_{11} . For the grid at $x = -6$ m the turbulence entering the contraction has relaxed to a practically isotropic state and thereafter attains a high degree of anisotropy from the straining in the contraction. For the grid at $x = -3.5$ m, i.e. positioned 0.5 m into the contraction, only a part of the total strain is acting on a then initially positive a_{11} -anisotropy. The variation of the degree of anisotropy at the beginning of the test section also depends on the turbulence Reynolds number which varies with the mean velocity.

The variation of the terms in the turbulent kinetic energy budget through the contraction is shown in figure 11. Here, the total dissipation is determined from the balancing method, and is seen to be about a factor of two smaller than the production during the rapidly straining phase. Hence, although the distortion is rapid in the middle part of the contraction, the dissipative terms are not negligible there. From the character of the variation of K through the contraction one can see that the average distortion is moderate.

The variation of the turbulent kinetic energy with downstream distance in the relaxation phase is shown in figure 12(a). The corresponding total dissipation rate, determined with the two methods described in §5.6, is shown in figure 12(b). The difference between the sum of all components (ε^T), equation (5.10), and the curve-fit method (ε^B), equation (5.14), is typically in the range 0% to 15%.

The corresponding variation of the different integral length scales is shown in figure 13. The largest integral scale is the one related to the transverse correlation along the axis of symmetry, \mathcal{A}_{vz} . This is in agreement with our intuitive understanding

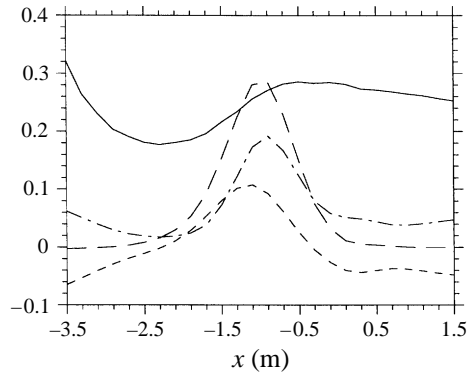


FIGURE 11. The turbulent kinetic energy together with the budget through the contraction and into the test section at $Re_T \sim 5000$. Solid line: $10K$, coarse-dashed line: production of K , dashed line: total derivative of K and chain-dashed line: total dissipation rate ε (all in SI-units).

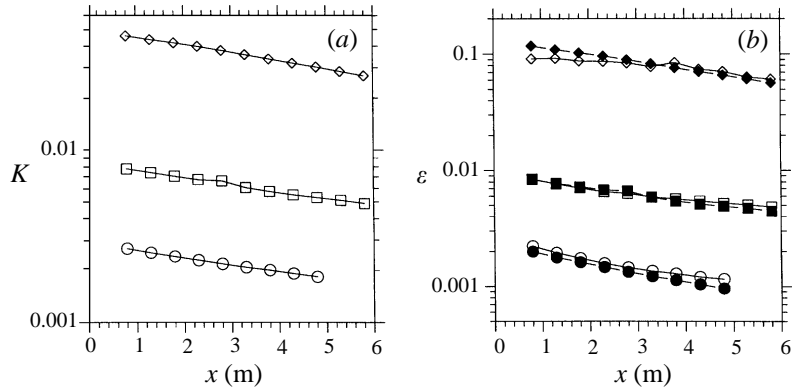


FIGURE 12. (a) Turbulent kinetic energy. (b) Total dissipation rate. Open symbols: ε^T , filled symbols: ε^B . See table 1 for symbols.

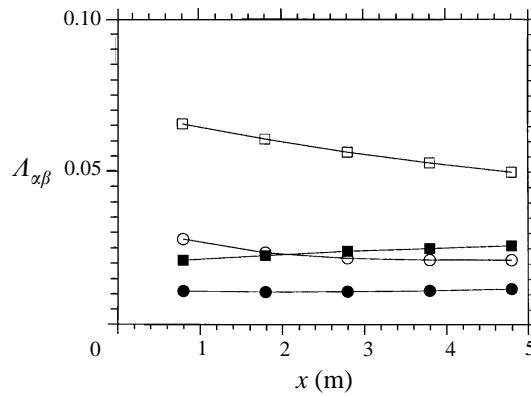


FIGURE 13. Integral lengthscales, $A_{\alpha\beta}$, versus downstream position from experiment E2a. \circ , A_{uz} ; \square , $A_{vz} = A_{wz}$; \bullet , A_{up} ; \blacksquare , A_{vp} .

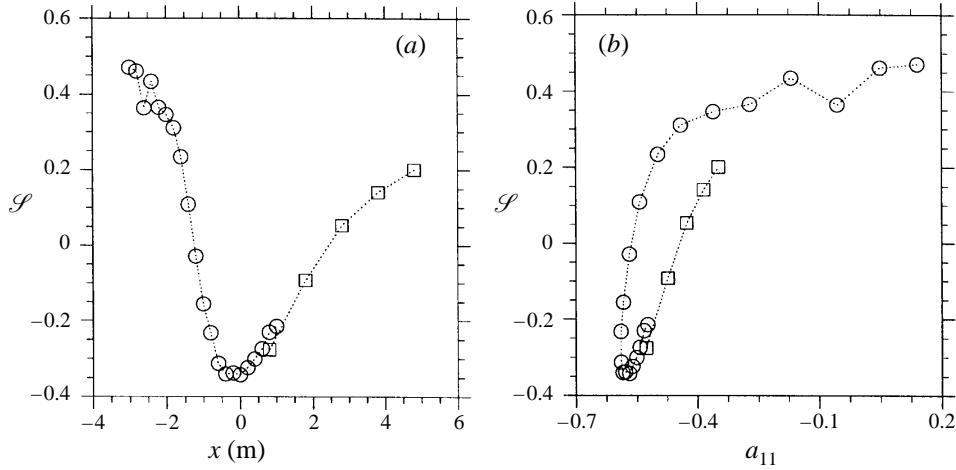


FIGURE 14. Velocity derivative skewness \mathcal{S} at $Re_T \sim 2000$. (a) Versus downstream distance. (b) Versus Reynolds stress anisotropy, a_{11} .

of vortex stretching along the direction of the axis of symmetry. The relaxation towards isotropy makes this lengthscale decrease in the test section, in sharp contrast to the standard behaviour in isotropic decaying turbulence.

6.1. Velocity derivative skewness

The statistical behaviour of the turbulent velocity for grid-generated turbulence has received considerable attention over the years. One of the quantities often used to characterize the turbulence is the velocity derivative skewness, \mathcal{S} , which is defined as

$$\mathcal{S} = \frac{\overline{(\partial u / \partial t)^3}}{\left[\overline{(\partial u / \partial t)^2} \right]^{3/2}} \quad (6.1)$$

and can be measured with the aid of a single hot-wire probe.

An experimental investigation of the different velocity derivative moments was made by Frenkiel & Klebanoff (1971) in isotropic grid-generated turbulence. They found that the velocity derivative skewness, \mathcal{S} , varied little with Reynolds number, $\mathcal{S} = (0.521, 0.493, 0.4)$ for $Re_\lambda = (37.7, 45.2, 60.8)$ respectively. Jiménez *et al.* (1993) made a numerical investigation of isotropic turbulence for Reynolds numbers $Re_\lambda = (35.1, 61.1, 94.1, 168.1)$ in which the velocity derivative skewness was found to be $\mathcal{S} = (0.49, 0.495, 0.52, 0.525)$ respectively.

Figure 14(b) clearly shows that the dependence of the velocity derivative skewness, \mathcal{S} , on the Reynolds stress anisotropy, a_{11} , is much stronger than on the Reynolds number. At $x \approx -3$ m where the turbulence is nearly isotropic and $Re_{\lambda_{uz}} = 80.7$, the measured value is $\mathcal{S} \approx 0.4$ which is in reasonable agreement with earlier results. Note that the velocity derivative skewness even changes sign for high anisotropies. This means for instance that one can no longer determine the time ‘direction’ of an arbitrary time signal with the aid of the velocity derivative skewness.

The strong variation with anisotropy is perhaps one explanation for the reversed Reynolds number trend found in the data of Frenkiel & Klebanoff (1971) compared with that of Jiménez *et al.* (1993). It is possible that the small variations in anisotropy

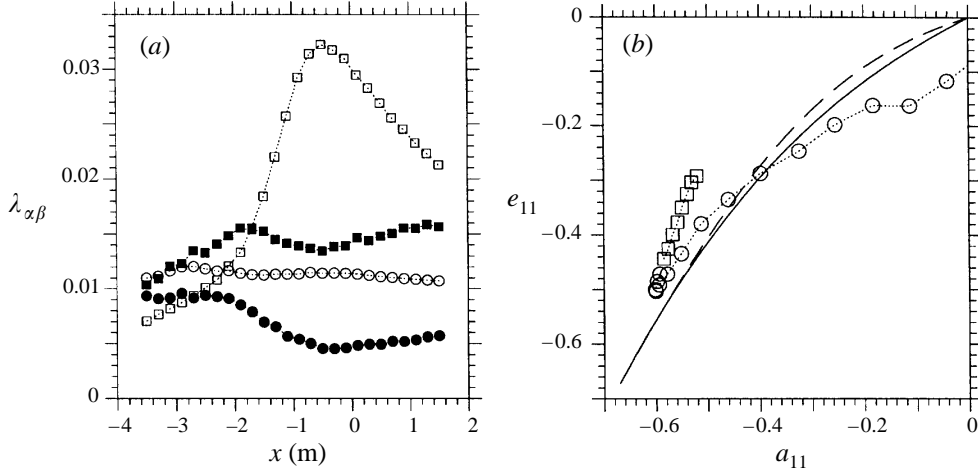


FIGURE 15. (a) The Taylor microscales (in m) versus downstream position. \circ , λ_{uz} ; \square , $\lambda_{vz} = \lambda_{wz}$; \bullet , λ_{up} ; \blacksquare , λ_{vp} . (b) The dissipation rate anisotropy: \circ , data from the straining part ($-4 < x < 0$); \square , data from the relaxation part ($x > 0$). Solid line: third-order model of Hallbäck *et al.* (1990). Dashed line: fifth-order model of Sjögren & Johansson (1997).

normally obtained from grid-generated turbulence can have affected the experimental results.

6.2. Dissipation rate anisotropy

The different Taylor microscales in the contraction and the early part of the test section can be seen in figure 15(a). In isotropic turbulence there is only one independent Taylor microscale, and the different scales are there related to each other by

$$\lambda_{uz} = \lambda_{vp} = \sqrt{2}\lambda_{vz} = \sqrt{2}\lambda_{up}. \quad (6.2)$$

These isotropic relations are essentially satisfied at $x \approx -3$ m. This is also in accordance with the fact that the Reynolds stresses are essentially equal at the same position as seen in figure 9(b).

Even though the turbulence Reynolds number is as high as $Re_T \approx 5000$ in this investigation the dissipation rate anisotropy becomes quite large in the straining phase of the contraction. This can occur since the non-dimensional mean strain rate is quite large (see discussion in connection with figure 9a).

The dissipation rate anisotropy has been determined from the relation

$$e_{11} = \frac{\varepsilon_{11}}{\varepsilon} - \frac{2}{3} = \frac{2}{1 + 2(\varepsilon_{22}/\varepsilon_{11})} - \frac{2}{3} \quad (6.3)$$

It is also seen in figure 15(b) that the dissipation rate anisotropy adheres reasonably well to the behaviour predicted by the model of Hallbäck *et al.* (1990). After the straining the return towards isotropy is somewhat faster than predicted by the model.

The Taylor microscales for the relaxation phase in the test section are shown in figure 16(a). The characteristic behaviour for the Taylor microscales in decaying isotropic turbulence is that they all increase. This is not the case here. The largest scales λ_{uz} and λ_{vz} decrease here as a result of the effects of intercomponent transfer. The turbulence Reynolds number is here $Re_T \approx 2000$ and the Taylor microscales exhibit a very different behaviour from that in isotropic turbulence in which they adhere to the relation (6.2) and increase monotonically.

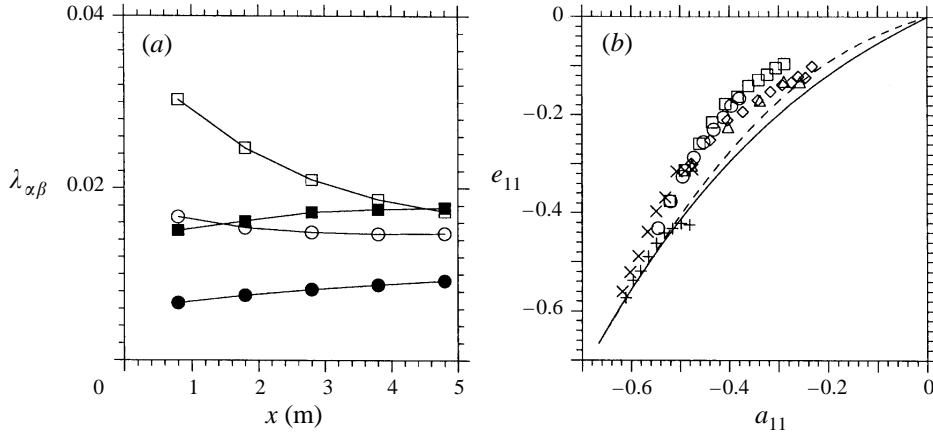


FIGURE 16. (a) Taylor microscales, $\lambda_{\alpha\beta}$, versus downstream position from experiment E2a. \circ , λ_{uz} ; \square , $\lambda_{vz} = \lambda_{wz}$; \bullet , λ_{up} ; \blacksquare , λ_{vp} . (b) Dissipation rate anisotropy, e_{11} , versus Reynolds stress anisotropy, a_{11} . Dashed line: fifth-order model by Sjögren & Johansson (1997), solid line: third-order model by Hallbäck *et al.* (1990). See table 1 for symbols.

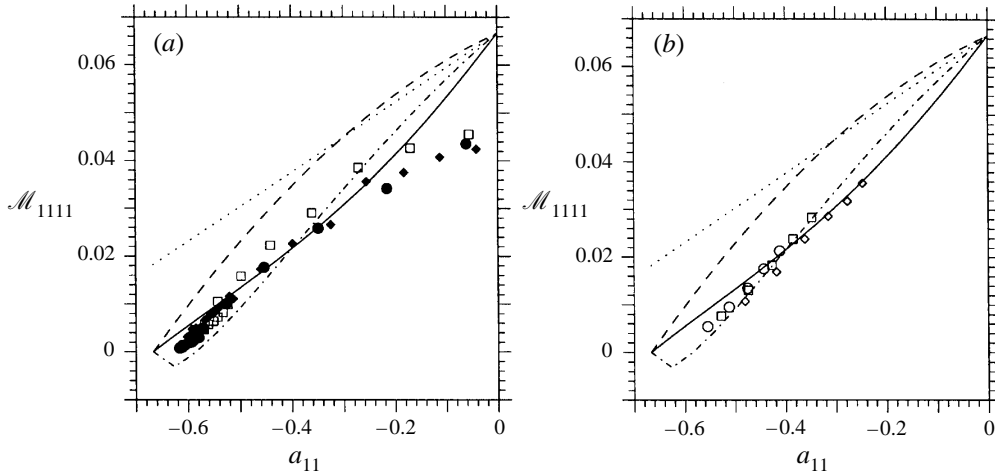


FIGURE 17. The non-dimensional fourth-order tensor component versus Reynolds stress anisotropy, which relates to the normalized rapid pressure-strain in axisymmetric turbulence as $\mathcal{M}_{1111} = \Pi_{11}^{(r)}/(12\sigma K)$. (a) Finite strain experiment, see table 2 for legend. (b) Return-to-isotropy experiment, see table 1 for symbols. Dotted line: linear model by Launder *et al.* (1975). Solid line and dashed line: fourth-order and second-order model respectively by Johansson & Hallbäck (1994). Chain-dashed line: Shih & Lumley (1985).

This difference in Taylor microscale behaviour is more clearly described by the dissipation rate anisotropy measure, e_{11} , shown in figure 16b. The data in figure 16(b) is a collection from all the different experiments compared with the third-order model of Hallbäck *et al.* (1990) and the fifth-order model of Sjögren & Johansson (1997). The dissipation rate anisotropy is more or less independent of the turbulence Reynolds number in the range spanned by the experiments, and is seen to be well described by both models. In general one should expect a trend of decreasing dissipation rate

anisotropy with increasing Reynolds number, but this variation is here essentially within the experimental uncertainty.

The difference between the third- and fifth-order model is quite small in homogeneous axisymmetric turbulence, but is much larger in other flows, e.g. in the vicinity of a wall, see Sjögren & Johansson (1997).

6.3. Rapid pressure–strain rate

With the method described in §3, the fourth-order tensor term, \mathcal{M}_{1111} (the integral in equation (3.8)), that multiplied by the mean velocity gradient tensor and the kinetic energy gives the rapid pressure–strain, can be determined in strained axisymmetric turbulence, and also in the absence of a mean strain. This quantity is shown in figure 17 in the contraction and in the subsequent relaxation ($x > 0$), and could be determined with high repeatability between different experiments. Comparisons are shown with the general linear ($C_2 = 0.4$) model of Launder, Reece & Rodi (1975) and nonlinear models of Shih & Lumley (1985) and (second and fourth order) of Johansson & Hallböck (1994). The second-order model of Johansson & Hallböck (1994) is equivalent with the model of Fu, Launder & Tselepidakis (1987) for irrotational mean flows. Further comparisons with other models and RDT in axisymmetric straining are given in Johansson & Hallböck (1994).

The fourth-order model is seen to give a good description of its behaviour for both parts. The integral (i.e. \mathcal{M}_{1111}) in equation (3.8) is determined from weighted quadrature of the two-point second-order velocity correlation $R_4 = \overline{uv'}$. This function can be seen in figure 18 for 12 different downstream positions.

The position of maximum strain rate in the contraction (see figure 9) is located at approximately $x = -1.1$ m, which is essentially at the same position, as seen from figure 18, as where the correlation function, R_4 , has its minimum. Consequently this is also the position where the integral, \mathcal{M}_{1111} , has its minimum value. The integral in equation (3.8) converges to within 90% if the domain is truncated at $\rho = 0.04$ m and $z = z_{max}/2$, which means that scatter in the integrand for large values of ρ and z has a very small influence on the total value of the integral \mathcal{M}_{1111} .

The results are shown in figure 19 in terms of the variation of the rapid pressure–strain rate, determined by use of equation (3.8). The repeatability of the results may be illustrated by the fact that the results in figure 19(b) originate from two different experiments, which were performed with over a year in between.

It is worth emphasizing that these are the first measurements presented in the literature to this date where the different parts of the pressure–strain have been obtained separately.

The comparison in figure 19 shows an excellent agreement with the nonlinear (fourth-order) model of Johansson & Hallböck (1994).

6.4. The budget

The total pressure–strain can be determined with good accuracy from balance in equation (1.6), giving the slow pressure–strain to total pressure–strain ratio as

$$\frac{\Pi_{11}^{(s)}}{\Pi_{11}} = 1 - \frac{\Pi_{11}^{(r)}}{\Pi_{11}}. \quad (6.4)$$

This non-dimensional quantity is shown in figure 20 versus the strain rate, σ . The names ‘slow’ and ‘rapid’ pressure–strain can be interpreted here. At the beginning of the contraction where the strain rate is low one could believe that the slow pressure–strain would contribute the major part of the total pressure–strain. This

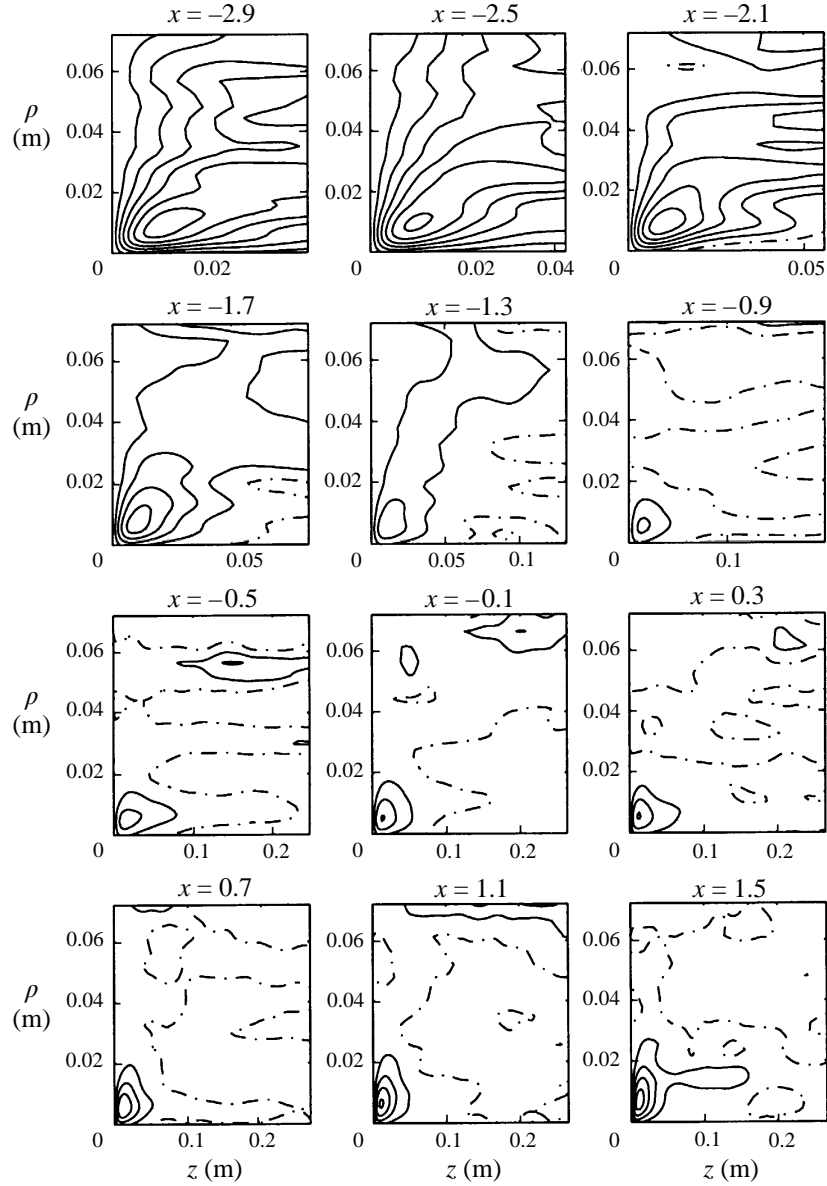


FIGURE 18. Two-point second-order correlation $R_4 = \overline{uv'}$ at different downstream locations. $u_r = (\overline{u^2})^{1/2}$, $v_r = (\overline{v^2})^{1/2}$. Contour increment 0.01. Chain-dashed line: zero contour. Solid line: positive contour.

is not the case seen from figure 20, where there is only rapid pressure-strain at the beginning of the contraction. It takes time (hence the name slow) for the triple correlations, which contribute to the slow pressure-strain, to develop. The second-order correlations, which determine the rapid pressure-strain, on the other hand, will immediately respond to the strain. This time lag in the slow pressure-strain rate cannot be captured by an algebraic model, which indicates a shortcoming in the second-order moment description of the slow pressure-strain.

The slow part always constitutes more than about 60% of the total pressure-strain at the position where the strain rate has its maximum value, signifying the importance

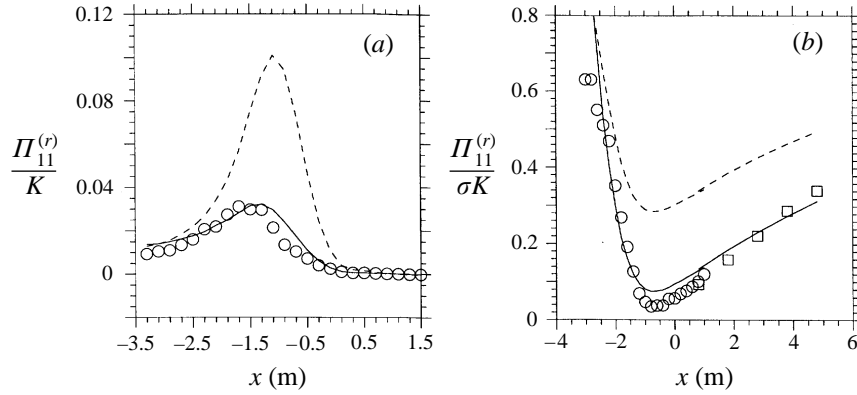


FIGURE 19. (a) Rapid pressure–strain vs. downstream distance at $Re_T \sim 5000$. Symbols: exp. results. Dashed line: linear model. Solid line: fourth-order model. (b) Rapid pressure–strain normalized with strain rate vs. downstream distance at $Re_T \sim 2000$. Symbols: exp. results. Dashed line: linear model. Solid line: fourth-order model.

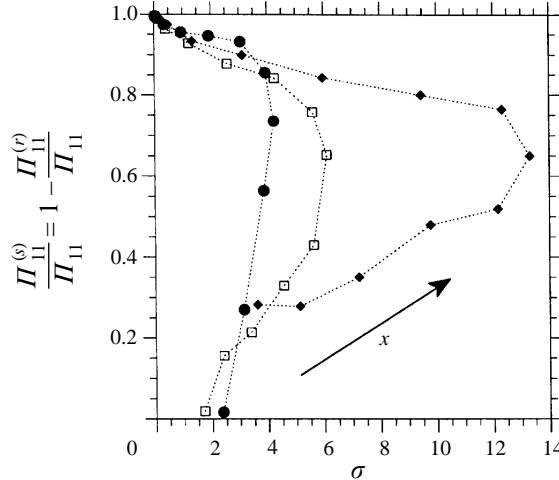


FIGURE 20. The slow pressure–strain to total pressure–strain ratio in the contraction versus the strain rate σ , with the down-stream position as a parameter ($-2 < x < 0$). See table 2 for symbols.

of the slow pressure–strain even in regions of rapid strain. This is somewhat analogous to the situation in the high-shear, near-wall region of turbulent boundary layers where the slow part actually dominates over the rapid pressure–strain.

Figure 21 shows the budget of (1.6) where all terms have been determined experimentally. The rapid part of the pressure–strain was measured directly with the aid of equation (3.8), and the slow part was here determined through balance of equation (1.6).

From figure 21 we again note that although the strain is quite rapid in the central part of the contraction the slow pressure–strain is comparable in magnitude to the rapid part. The effects caused by the difference in anisotropy between the stress and the dissipation rate, see equation (1.6), are quite small.

6.5. Slow pressure–strain rate

The slow pressure–strain can be determined by use of equation (5.17) with the probes mounted in a VV-configuration. Using equation (4.4) we can evaluate an effective

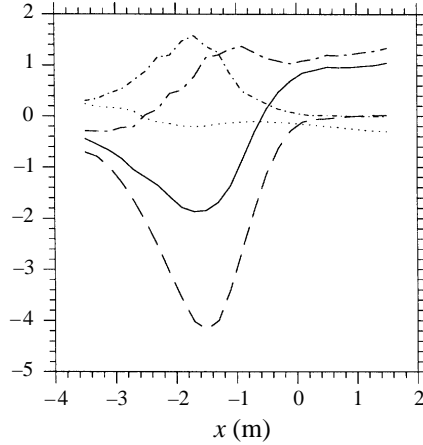


FIGURE 21. Reynolds stress anisotropy (a_{11}) budget. The full line represents the left-hand side of (1.6). The right-hand side contains production (dashed), rapid pressure-strain (chain-dashed), slow pressure-strain (coarse chain-dashed) and the difference in anisotropy between the stress and the dissipation rate (dotted).

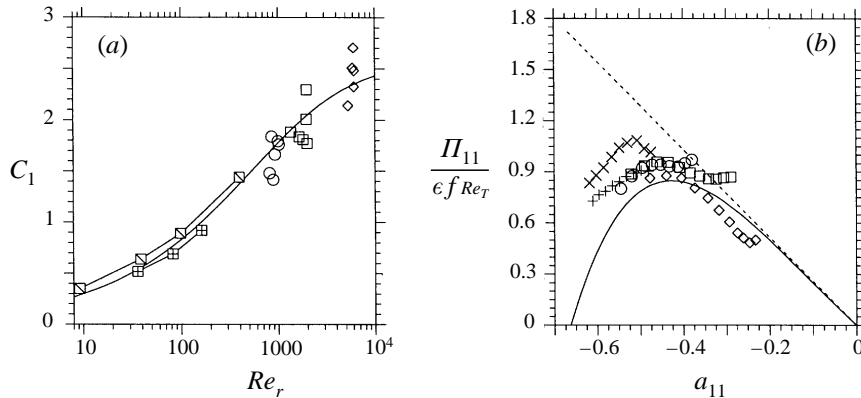


FIGURE 22. (a) The Rotta constant C_1 as a function of the turbulence Reynolds number Re_T from different realizations in relaxing anisotropic axisymmetric turbulence. Filled squares represent DNS data from Hallbäck (1993). See table 1 for other symbols. Solid curve represents the model expression (4.5). C_1 was evaluated in the experiments for $a_{11} = -0.4$ and in DNS for $a_{11} = -0.38$ and $a_{11} = -0.30$. (b) Amplitude variation of the normalized slow pressure-strain, $\Pi_{ij}^{(s)}/(\epsilon f Re_T)$. Solid curve model of Sjögren & Johansson (1997). $c_1 = -2.4, c_2 = 2.2$ and $c_3 = 1.2$. Dashed line: linear Rotta model with $C_1 = C_{1\infty} f(Re_T)$, $C_{1\infty} = 2.58$. See table 1 for other symbols.

Rotta constant. The resulting experimental values are shown in figure 22(a) versus the Reynolds number, and are compared there with DNS data of Hallbäck *et al.* (1993). Also included is the model proposed by Hallbäck *et al.* (1993) which is seen to capture the Reynolds number variation quite well over the whole range of Reynolds numbers which spans several decades.

The normalized slow pressure-strain, $\Pi_{ij}^{(s)}/(\epsilon f Re_T)$, is shown as a function of the Reynolds stress anisotropy, a_{11} , in figure 22(b). It is compared with the linear Rotta model with a Reynolds number dependent Rotta constant, and with the fifth-order model of Sjögren & Johansson (1997). The linear Rotta model fails to predict the normalized pressure-strain at high anisotropies, whereas the realizable fifth-order

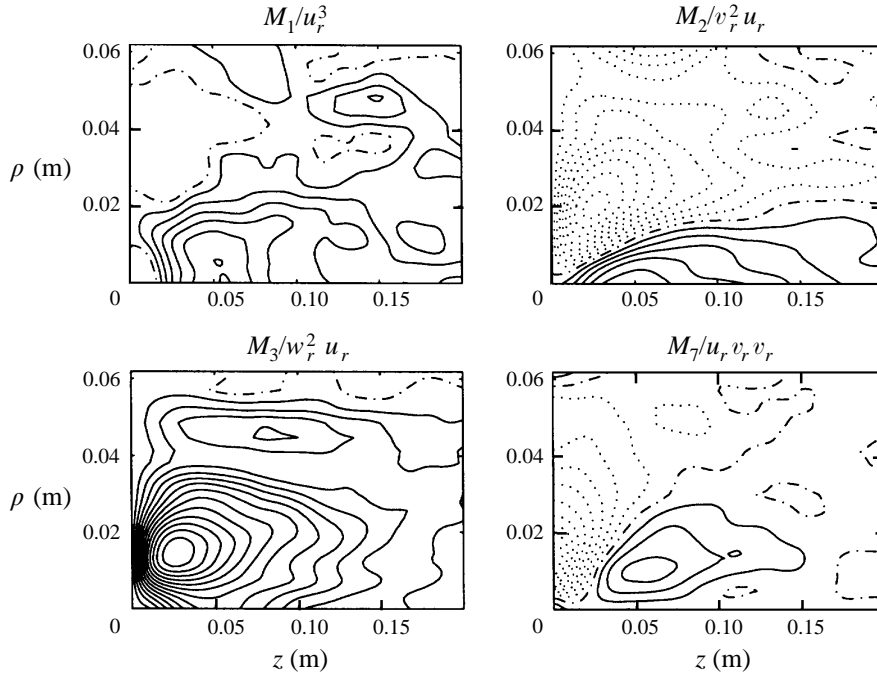


FIGURE 23. Normalized M -functions determined with two X-probes in turbulence with high degree of anisotropy, $a_{11} = -0.53$. (Contour increment 0.005). $u_r = (\overline{u^2})^{1/2}$, $v_r = (\overline{v^2})^{1/2}$, $w_r = (\overline{w^2})^{1/2}$.

model captures the overall behaviour at all anisotropies. Sjögren & Johansson (1997) have also shown that the fifth-order model predicts the slow-pressure-strain rate reasonably well over essentially the entire Reynolds stress anisotropy invariant map. Other nonlinear models have been proposed by e.g. Shih (1995) and Launder (1995) (see respective chapters in Hallböck *et al.* 1995), but these models describe the total return-to-isotropy term. Complete RST-models and their performance, not only in axisymmetric turbulence but also in more complex flows, are discussed and analysed in some detail in Sjögren & Johansson (1997).

The slow pressure-strain can also be determined using equation (3.9) with the probes mounted in a VW-configuration. This method requires much more work since the integral of equation (3.9) contains four different two-point third-order velocity correlations which have to be determined. These correlations can be seen in figure 23 for a case with high degree of anisotropy, at the beginning of the relaxation phase.

A large amount of data is needed to obtain well-defined triple-correlations. This is particularly obvious for large separations which is seen in figure 23. However, the largest separations are not very important since the pressure-strain can be calculated with good accuracy (90%), by truncating the integration at $z = 0.1$ m and $\rho = 0.03$ m.

Figure 24 shows a comparison between the two different methods described by equation (5.17) and equation (3.9), the balancing method and the direct method respectively, for three different turbulence Reynolds numbers. The balancing method proved to give a somewhat higher degree of repeatability. One explanation of the somewhat higher scatter in the data determined directly would be that the direct method, which involves third-order correlations, requires a longer total sampling time in order to achieve the same statistical accuracy compared to the second-order correlations, which are needed for the balancing method.

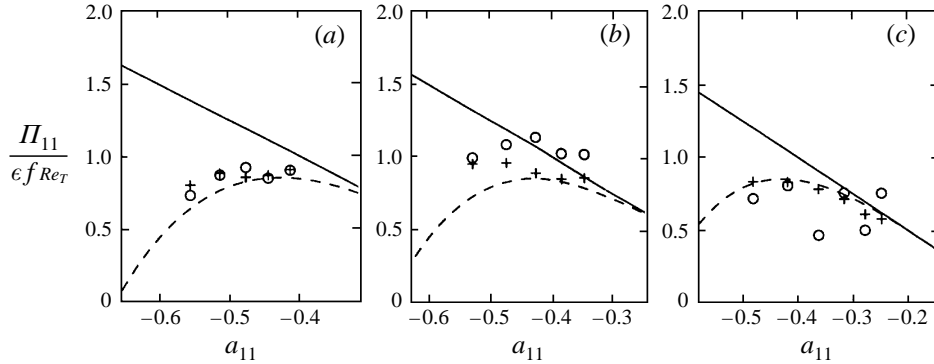


FIGURE 24. Slow pressure–strain rate for $Re_T = (1000, 2000, 5000)$ (a–c). The balancing method (+) equation (5.17) and the direct method (o) equation (3.9). Solid line: linear Rotta model with $C_1 = C_{1\infty}f(Re_T)$, $C_{1\infty} = 2.58$. Dashed curve: model of Sjögren & Johansson (1997), $c_1 = -2.4$, $c_2 = -2.2$ and $c_3 = 1.2$.

One should point out that a direct determination of the pressure–strain rate (without balancing it out from the Reynolds stress equations) has never previously been reported, and makes it possible to separately determine the slow and rapid parts in the case of strained homogeneous axisymmetric turbulence.

7. Concluding remarks

Initially nearly isotropic turbulence was subjected to an axisymmetric strain generated by a contraction in a wind tunnel. The non-dimensional maximum mean strain rate (normalized by K/ϵ) could be varied in the experiments up to values where a behaviour close to that described by RDT is achieved in parts of the contraction. It was demonstrated that the rapid part of the pressure–strain could be accurately determined from measurements of second-order two-point velocity correlations. The fact that this could be achieved even in the situations in which the rapid and slow parts are of similar magnitude opens up new possibilities for detailed testing of pressure strain rate models using experimental data. The realizable fourth-order model for the rapid pressure–strain by Johansson & Hallbäck (1994) was shown to accurately describe its behaviour.

It was shown that both the return timescales τ_{r_1} and τ_{r_2} for the second and the third invariants of the Reynolds stress anisotropy tensor are important quantities in the analysis of the ‘return-to-isotropy’ process of homogeneous turbulence. The return process is driven by both viscous and pressure related effects and is very difficult to analyse with knowledge of only the evolution of the Reynolds stress tensor. The split of the return-to-isotropy tensor into two parts, the dissipation rate anisotropy tensor and the slow pressure–strain tensor, was shown to be a good choice since the dissipation rate anisotropy tensor showed a very weak turbulence Reynolds number dependence and was very well described by a nonlinear algebraic realizable model. The slow pressure–strain exhibited both a turbulence Reynolds number dependence which could reasonably well be described by the model of Hallbäck *et al.* (1993) and a dependence on the degree of Reynolds stress anisotropy which could be captured by a nonlinear algebraic realizable model.

The newly developed theory of Lindborg (1995) for the kinematics of homogeneous axisymmetric turbulence was shown to be of great experimental importance, leading to a technique which allows the pressure–strain rate terms to be determined directly.

We wish to thank Dr Magnus Hallbäck and Dr Erik Lindborg for many interesting discussions on the present topic and the latter for making experiments in homogeneous axisymmetric turbulence more attractive by contribution of new theoretical results. We also wish to thank Jens Österlund for all help and support with work connected to the MTL wind-tunnel. This research was supported by TFR.

REFERENCES

- ALVELIUS, K., HALLBÄCK, M. & JOHANSSON, A.V. 1997 Calibration of models for the slow pressure-strain using LES. *Turbulent Shear Flows XI, Grenoble, Sept., 1997*, P2:107–112. Springer.
- BATCHELOR, G. K. 1946 The theory of axisymmetric turbulence. *Proc. R. Soc. Lond. A* **186**, 480–502.
- BATCHELOR, G. K. 1953 *The Theory of Homogeneous Turbulence*. Cambridge University Press.
- BATCHELOR, G. K. & TOWNSEND, A. A. 1947 Decay of vorticity in isotropic turbulence. *Proc. R. Soc. Lond. A* **190**, 534–550.
- BATCHELOR, G. K. & TOWNSEND, A. A. 1948 Decay of isotropic turbulence in the initial period. *Proc. R. Soc. Lond. A* **192**, 539–558.
- CAMBON, C., JACQUIN, L. & LUBRANO, J. L. 1992 Toward a new Reynolds stress model for rotating turbulent flows. *Phys. Fluids A* **4**, 812–824.
- CAMBON, C., MANSOUR, N. N. & GODEFERD, F. S. 1997 Energy transfer in rotating turbulence. *J. Fluid Mech.* **337**, 303–332.
- CHANDRASEKHAR, S. 1950 The theory of axisymmetric turbulence. *Phil. Trans. R. Soc. Lond. A* **242**, 557–577.
- CHOI, K.-S. 1983 A study of the return to isotropy of homogeneous turbulence. PhD Thesis, Cornell University.
- COMTE-BELLOT, G. & CORRSIN, S. 1966 The use of a contraction to improve the isotropy of grid-generated turbulence. *J. Fluid Mech.* **25**, 657–682.
- FRENKIEL, F. N. & KLEBANOFF, P. S. 1971 Statistical properties of velocity derivatives in a turbulent field. *J. Fluid Mech.* **48**, 183–208.
- FU, S., LAUNDER, B. E. & TSELEPIDAKIS D. P. 1987 Accommodating the effect of high strain rates in modeling the pressure-strain correlation. *UMIST Mech. Engng Dep Rep.* TFD/87/5.
- GENCE, J. N. & MATHIEU, J. 1980 The return to isotropy of homogeneous turbulence having been submitted to two successive plane strains. *J. Fluid Mech.* **101**, 555–566.
- GEORGE, W. & HUSSEIN, H. J. 1991 Locally axisymmetric turbulence. *J. Fluid Mech.* **233**, 1–23.
- GRANT, H. L. & NISBET, I. C. T. 1957 The inhomogeneity of grid turbulence. *J. Fluid Mech.* **2**, 263–272.
- GROTH, J., HALLBÄCK, M. & JOHANSSON, A. V. 1989 Measurement and modelling of anisotropic turbulent flows. In *Advances in Turbulence*, vol. 2, p. 84 (ed. H. Fernholz & H. Fiedler). Springer.
- HALLBÄCK, M. 1993 Development of Reynolds stress closures of homogeneous turbulence through physical and numerical experiments. PhD thesis, Dept. of Mech., KTH, Stockholm.
- HALLBÄCK, M., GROTH, J. & JOHANSSON, A. V. 1990 An algebraic model for nonisotropic turbulent dissipation rate term in Reynolds stress closures. *Phys. Fluids A* **2**, 1859–1866.
- HALLBÄCK, M., HENNINGSON, D., JOHANSSON, A. V. & ALFREDSON, P. H. (Eds.) 1995 *Turbulence and Transition Modelling* 1995 Lecture Notes from the ERCOFTAC/IUTAM Summer School in Stockholm 12–20 June, 1995, ERCOFTAC Series, vol. 2. Kluwer.
- HALLBÄCK, M., SJÖGREN, T. & JOHANSSON, A. V. 1993 Modelling of intercomponent transfer in Reynolds stress closures of homogeneous turbulence. In *Turbulent Shear Flows IX* (ed. F. Durst, Kasagi, B. Launder & J. Whitelaw), pp. 21–31. Springer.
- HARRIS, V. G., GRAHAM, J. A. H. & CORRSIN, S. 1977 Further experiments in nearly homogeneous turbulent shear flow. *J. Fluid Mech.* **81**, 657–687.
- HINZE, J. O. 1975 *Turbulence*. McGraw-Hill.
- HUSSAIN, A. K. M. F. & RAMJEE, V. 1976 Effect of the axisymmetric contraction shape on incompressible turbulent flow. *Trans. ASME: J. Fluids Engng* **98**, 58–69.
- JIMÉNEZ, J., WRAY, A. A., SAFFMAN, P. G. & ROGALLO, R. S. 1993 The structure of intense vorticity in isotropic turbulence. *J. Fluid Mech.* **225**, 65–90.

- JOHANSSON, A. V. 1992 A low-speed wind-tunnel with extreme flow quality – design and tests. *Proc. of the 18th ICAS Congress*, Paper ICAS-92-3.8.1.
- JOHANSSON, A. V. 1995 The hierarchy of one-point closures and the modelling of rotational effects. In *Advances in Turbulence V* (ed. R. Benzi), pp. 251–255. Kluwer.
- JOHANSSON, A. V. & HALLBÄCK, M. 1994 Modelling of rapid pressure–strain in Reynolds-stress closures. *J. Fluid Mech.* **269**, 143–168, and Corrigendum **290**, 405.
- KÁRMÁN, T. VON & HOWARTH, L. 1938 On the statistical theory of isotropic turbulence. *Proc. R. Soc. Lond. A* **164**, 192–215.
- KASSINOS, S. C. & REYNOLDS, W. C. 1994 A structure-based model for the rapid distortion of homogeneous turbulence. Report TF-61, Thermosciences Division, Dept. of Mechanical Engineering, Stanford Univ.
- LAUNDER, B. E., REECE, G. J. & RODI, W. 1975 Progress in the development of a Reynolds stress turbulence closure. *J. Fluid Mech.* **68**, 537–566.
- LEE, M. J. & REYNOLDS, W. C. 1985 Numerical experiments on the structure of homogeneous turbulence. *Stanford Univ., Dept. of Mech. Eng.*, Rep. TF-24.
- LE PENVEN, L., GENCE, J. N. & COMTE-BELLOT, G. 1985 On the approach to isotropy of homogeneous turbulence: effect of the partition of kinetic energy among the velocity components. In *Frontiers in Fluid Mechanics* (ed. S. H. Davis & J. L. Lumley). Springer.
- LEUCHTER, O. & CAMBON, C. 1997 EDQNM and DNS predictions of rotating effect in strained axisymmetric turbulence. In *Proc. Eleventh Turbulent Shear Flows Conf., Grenoble, Sept. 1997*: 31: pp. 7–12.
- LEUCHTER, O. & DUPEUBLE, A. 1993 Rotating homogeneous turbulence subjected to a axisymmetric contraction. In *Proc. Ninth Turbulent Shear Flows Conf., Kyoto, August 1993*. 137: pp. 1–6.
- LINDBORG, E. 1995 Kinematics of homogeneous axisymmetric turbulence. *J. Fluid Mech.* **302**, 179–201.
- LUMLEY, J. L. & NEWMAN, G. R. 1977 The return to isotropy of homogeneous turbulence. *J. Fluid Mech.* **82**, 161–178.
- MANSOUR, N. N., KIM, J. & MOIN, P. 1988 Reynolds-stress and dissipation-rate budgets in a turbulent channel flow. *J. Fluid Mech.* **194**, 15–44.
- PRANDTL, L. 1930 *The Physics of Solids and Fluids*. Blackie.
- RISTORCELLI, J. R., LUMLEY, J. L. & ABID, R. 1995 A rapid-pressure covariance representation consistent with the Taylor-Proudman theorem materially frame indifferent in the two-dimensional limit. *J. Fluid Mech.* **292**, 111–152.
- ROTTA, J. 1951 Statistische theorie nichthomogener turbulenz I. *Z. Physik.* **129**, 547–572.
- SCHUMANN, U. 1977 Reliability of Reynolds stress turbulence models. *Phys. Fluids* **20**, 721–725.
- SHIH, T. H. & LUMLEY, J. L. 1985 Modeling of pressure correlation terms in Reynolds stress and scalar flux equations. *Sibley School Mech. and Aerospace Engng Rep. FDA-85-3*. Cornell University.
- SIMMONS, L. F. G. & SALTER, C. 1934 Experimental investigation and analysis of the velocity variations in turbulent velocity field. *Proc. R. Soc. Lond. A* **145**, 212–234.
- SJÖGREN, T. & JOHANSSON, A. V. 1994 Measurement and modelling of anisotropic dissipation and slow pressure–strain in homogeneous turbulence. In *Advances in Turbulence V* (ed. R. Benzi), pp. 486–490. Kluwer.
- SJÖGREN, T. & JOHANSSON, A. V. 1997 Development and calibration of algebraic nonlinear models for terms in the Reynolds stress transport equations. *Phys. Fluids* (submitted).
- SPEZIALE, C. G., SARKAR, S. & GATSKI, T. B. 1991 Modelling the pressure–strain correlation of turbulence: an invariant dynamical system approach. *J. Fluid Mech.* **227**, 245–272.
- TAYLOR, G. I. 1935a Turbulence in a contracting stream. *Z. Angew. Math. Mech.* **15**, 91–96.
- TAYLOR, G. I. 1935b Statistical theory of turbulence, parts I and II. *Proc. R. Soc. Lond. A* **151**, 421–454.
- TUCKER, H. J. & REYNOLDS, A. J. 1968 The distortion of turbulence by irrotational plane strain. *J. Fluid Mech.* **32**, 657–673.
- UBEROI, M. S. 1956 Effect of wind-tunnel contraction on free-stream turbulence. *J. Aero. Sci.* **23**, 754–764.
- UBEROI, M. S. 1957 Equipartition of energy and local isotropy in turbulent flows. *J. Appl. Phys.* **28**, 1165–1170.
- WARHAFT, Z. 1980 An experimental study of the effect of uniform strain on thermal fluctuations in grid-generated turbulence. *J. Fluid Mech.* **99**, 545–573.